2007-12

High doppler resolution imaging by multistatic continuous wave radars using constructive techniques

Soh, Wei Ting

Monterey California. Naval Postgraduate School

NAVAL POSTGRADUATE SCHOOL

MONTEREY, CALIFORNIA

THESIS

HIGH DOPPLER RESOLUTION IMAGING BY MULTISTATIC CONTINUOUS WAVE RADARS USING CONSTRUCTIVE TECHNIQUES

by

Wei Ting Soh

December 2007

Thesis Advisor:	Brett Borden
Second Reader:	Donald Walters

Approved for public release; distribution is unlimited

THIS PAGE INTENTIONALLY LEFT BLANK

REPORT DOCUMENTATION PAGE			*Form Approved OMB No. 0704-0188*
Public reporting burden for this collection of information is estimated to average 1 hour per response, including the time for reviewing instruction, searching existing data sources, gathering and maintaining the data needed, and completing and reviewing the collection of information. Send comments regarding this burden estimate or any other aspect of this collection of information, including suggestions for reducing this burden, to Washington headquarters Services, Directorate for Information Operations and Reports, 1215 Jefferson Davis Highway, Suite 1204, Arlington, VA 22202-4302, and to the Office of Management and Budget, Paperwork Reduction Project (0704-0188) Washington DC 20503.			
1. AGENCY USE ONLY ***(Leave blank)***	**2. REPORT DATE** December 2007	**3. REPORT TYPE AND DATES COVERED** Master's Thesis	
4. TITLE AND SUBTITLE High Doppler Resolution Imaging by Multistatic Continuous Wave Radars Using Constructive Techniques			**5. FUNDING NUMBERS**
6. AUTHOR(S) Wei Ting Soh			
7. PERFORMING ORGANIZATION NAME(S) AND ADDRESS(ES) Naval Postgraduate School Monterey, CA 93943-5000			**8. PERFORMING ORGANIZATION REPORT NUMBER**
9. SPONSORING /MONITORING AGENCY NAME(S) AND ADDRESS(ES) N/A			**10. SPONSORING/MONITORING AGENCY REPORT NUMBER**
11. SUPPLEMENTARY NOTES The views expressed in this thesis are those of the author and do not reflect the official policy or position of the Department of Defense or the U.S. Government.			
12a. DISTRIBUTION / AVAILABILITY STATEMENT Approved for public release; distribution in unlimited			**12b. DISTRIBUTION CODE**

13. ABSTRACT (maximum 200 words)

The multistatic radar offers many advantages over monostatic radar in certain applications, especially since the receiving stations may be located at covert and distant sites relative to the transmitting stations. Furthermore, continuous wave radars are relatively simple and inexpensive to employ and maintain. Hence, the impetus for developing a CW multistatic radar system for high-resolution imaging was conceived.

This thesis is a proof of concept demonstration that a Doppler-only multistatic radar system can be employed to provide high resolution imaging of airborne targets in support of non-cooperative target recognition. Through an understanding of conventional imaging techniques and formulation of the inverse problem in radar imaging, a demonstration radar model based on one transmitter and two receivers was designed to determine the accurate position and velocity of simulated targets. The extraction errors resulted from the range, bearing and velocity measurements were congruent with the physical limitations of each transmitter-receiver pair. Through the employment of a multistatic system, the geometrical diversity allowed these limitations to be overcome.

14. SUBJECT TERMS High Doppler Resolution, Radar Imaging, Multistatic, Bistatic			**15. NUMBER OF PAGES** 95
			16. PRICE CODE
17. SECURITY CLASSIFICATION OF REPORT Unclassified	**18. SECURITY CLASSIFICATION OF THIS PAGE** Unclassified	**19. SECURITY CLASSIFICATION OF ABSTRACT** Unclassified	**20. LIMITATION OF ABSTRACT** UU

NSN 7540-01-280-5500 Standard Form 298 (Rev. 2-89)
Prescribed by ANSI Std. 239-18

THIS PAGE INTENTIONALLY LEFT BLANK

Approved for public release; distribution is unlimited

HIGH DOPPLER RESOLUTION IMAGING BY MULTISTATIC CONTINUOUS WAVE RADARS USING CONSTRUCTIVE TECHNIQUES

Wei Ting Soh
Major, Republic of Singapore Air Force
Bachelor of Engineering (EEE), Nanyang Technological University, 2001

Submitted in partial fulfillment of the
requirements for the degree of

**MASTER OF SCIENCE IN
COMBAT SYSTEMS SCIENCES AND TECHNOLOGY**

from the

**NAVAL POSTGRADUATE SCHOOL
December 2007**

Author: Wei Ting Soh

Approved by: Professor Brett Borden
Thesis Advisor

Professor Donald Walters
Second Reader

Professor James Luscombe
Chairman, Department of Physics

THIS PAGE INTENTIONALLY LEFT BLANK

ABSTRACT

The multistatic radar offers many advantages over monostatic radar in certain applications, especially since the receiving stations may be located at covert and distant sites relative to the transmitting stations. Furthermore, continuous wave radars are relatively simple and inexpensive to employ and maintain. Hence, the impetus for developing a CW multistatic radar system for high-resolution imaging was conceived.

This thesis is a proof of concept demonstration that a Doppler-only multistatic radar system can be employed to provide high resolution imaging of airborne targets in support of non-cooperative target recognition. Through an understanding of conventional imaging techniques and formulation of the inverse problem in radar imaging, a demonstration radar model based on one transmitter and two receivers was designed to determine the accurate position and velocity of simulated targets. The extraction errors resulted from the range, bearing and velocity measurements were congruent with the physical limitations of each transmitter-receiver pair. Through the employment of a multistatic system, the geometrical diversity allowed these limitations to be overcome.

THIS PAGE INTENTIONALLY LEFT BLANK

TABLE OF CONTENTS

LIST OF FIGURES

THIS PAGE INTENTIONALLY LEFT BLANK

LIST OF TABLES

THIS PAGE INTENTIONALLY LEFT BLANK

ACKNOWLEDGMENTS

I would like to express my deep and sincere gratitude to my thesis advisor, Professor Brett Borden. His understanding, encouragement and personal guidance provided a good basis for this thesis. His critical ideas and patience in working with me on an outline made the forging of this thesis possible. His extensive knowledge and logical way of thinking have been of great value to me, especially during those periods when I seemed to have reached a dead-end in my research. This work would not have been possible if not for his professional and personal attention.

I also wish to express my warm and sincere thanks to my thesis co-advisor, Professor Donald Walters. His recommendations have been very welcoming and quite insightful to my understanding of the research topics.

I especially want to thank my colleague and friend in the inverse scattering laboratory, LT Armando Lucrecio. His kind assistance and tips on the use of Apple computers facilitated my smooth initiation into the laboratory. His knowledge in radar imaging and digital signal processing provided valuable insights into my research. His friendship and encouragement motivated me to persevere in times of difficulty.

Finally, I want to give special thanks to my lovely wife, Sheau Shyuan. It has been a difficult year for her, especially since she has to look after our newborn daughter Yenn Shan, in Singapore while I endeavored to complete my research in Monterey. Without her understanding and support, it would have been impossible for me to finish this work.

THIS PAGE INTENTIONALLY LEFT BLANK

I. INTRODUCTION

A. DOPPLER-ONLY MULTISTATIC RADAR IMAGING

IEEE Standard 686-1997 [1] defined the multistatic radar as a radar system having two or more transmitting or receiving antennas with all antennas separated by large distances when compared to the antenna sizes. It has at least three components — for instance, one transmitter and two receivers, or multiple receivers and multiple transmitters. It is a generalization of the bistatic radar system, with one or more receivers processing echo field returns from one or more geographically separated transmitters. The multistatic radar system is desirable as it allows covert operation of the receivers and there is increased resilience to electronic countermeasures. Additionally, due to geometrical effects, the radar cross-section of the target could potentially be enhanced.

Conventional synthetic aperture radar or inverse synthetic aperture radar imaging involves the processing of short pulse signals to form high range resolution images of the target. Similarly, high Doppler resolution data could be utilized to generate images. One major benefit of employing high Doppler resolution imaging in a multistatic radar system is the requirement for relatively simple and inexpensive continuous wave (CW) transmitters and receivers. For a typical airborne target, the signal returns are intrinsically considered narrowband since the Doppler shifts are usually in the region of tens to hundreds of kilohertz. This narrowband attribute in a Doppler imaging system has utility in operations where the available frequency spectrum is limited.

Conceptually, a Doppler-only multistatic radar system could potentially provide high-resolution imaging of airborne targets in support of non-cooperative target recognition [2], while keeping the cost and ease of implementation and maintenance to a significantly lower level when compared with current pulse-Doppler monostatic radars. This is the subject of this thesis.

B. OBJECTIVE

The objective of this thesis is to develop a basic theory for a Doppler-only multistatic radar system based on high-Doppler resolution data. The physics involved in resolving the geometry of the targets relative to the transmitters and receivers, as well as the imaging process will be discussed. The mathematical implementation of such a radar system will also be examined. Thereafter, the results of the above analysis will be exercised on test cases.

C. THESIS ORGANIZATION

The thesis is divided into eight chapters, organized as follows.

Chapter II provides a review of current imaging methods, including one-dimensional high range resolution imaging, its extension to two-dimensional imaging, and high Doppler resolution imaging.

Chapter III provides some background of inverse problems in radar imaging. The well-posedness and condition number of the problem, and the method of least squares are discussed.

Chapter IV introduces the concepts of bistatic radars. It presents an overview of bistatic radar definitions and the parameters involved in the derivation of the model. Thereafter, it extends the bistatic model into the multistatic case. The advantages and disadvantages of the multistatic radar, as well as the implementation requirements, are discussed.

Chapter V introduces the design of the radar model. It describes the mathematical approach to derive the target's position and velocity.

Chapter VI involves the implementation of the multistatic radar model for imaging. It illustrates the results and tabulation of measurement errors.

Chapter VII provides the results analysis and an examination of the imaging artifacts.

Finally, Chapter VIII recommends areas of future work and concludes with some comments on the impetus towards developing a Doppler-only multistatic radar system.

THIS PAGE INTENTIONALLY LEFT BLANK

II. RADAR IMAGING METHODS

A. OVERVIEW OF IMAGING RADAR

Radar systems measure the strength of the backscatter and the round trip delay time of radio frequency signals reflected from distant objects. Since the radar pulse travels at the speed of light, it is relatively straightforward to use the measured time delay for the round trip of a particular pulse to calculate the range to the reflecting object. The resolution in the down-range direction is governed by the pulse bandwidth: a higher bandwidth will imply finer resolution in this direction. The resolution of the image in the cross-range direction is determined by the dimensions of the radar antenna and a larger antenna will lead to finer resolution in the azimuth direction.

This chapter discusses the current imaging methods such as one-dimensional high range resolution (HRR) imaging, two-dimensional imaging and high Doppler resolution (HDR) imaging will be discussed.

B. ONE-DIMENSIONAL IMAGING

One-dimensional imaging involves the generation of range profiles, which is a straightforward method of articulating target substructure. High range resolution imaging involves the resolution of the individual target scatterers through the down-range profile of the target. This method essentially provides a one-dimensional image of the target and an example is shown in Figure 1. Short pulse or pulse-compressed signals can be used to form one-dimensional HRR images of the target. As the short pulse sweeps across the target, it sequentially excites the scatterers on the target, which re-radiate energy back to the radar receiver. When these scatterers are non-interacting and point-like, the scattered pulse will be a sum of damped and blurred images of the incident pulse, which are shifted by time delays that are proportional to the scatterer's range [3]. For pulse compression, the two common waveforms are linear frequency modulation and binary phase coded pulses [4].

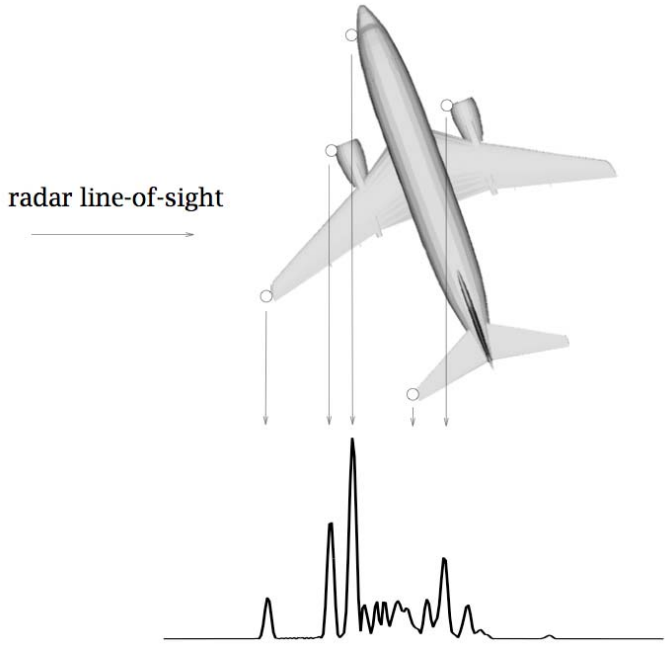

Figure 1. Example of a range profile of a Boeing 737-500 (From [5])

The down-range profile can be affected by a variety of factors such as target aspect angle, position of the scatterers or masking of scatterers by other parts of the target. Additionally, since the bandwidth of a pulse is inversely proportional to its duration, the use of short pulses will lead to large bandwidth requirements. Wide bandwidth can increase system complexity and increase the likelihood of interference from other emitters in the electromagnetic spectrum. A short-pulse waveform also provides less accurate radial velocity measurement as compared to that obtained from Doppler frequency shift. As high peak power is required to transmit short pulses over long ranges, it is an important limitation in radar applications. High peak power transmission can result in voltage breakdown, especially at high frequencies since the waveguide dimensions are small.

Radar imaging through using only range profiles has limited applications. This is due to the fact a range profile will not be able to distinguish cross-range target structures. All scatterers located at the same distance from the radar will reflect energy back to the radar with the same time delay. Hence, when the radar illuminates many distinct targets

at any instant, conclusive decisions pertaining to the nature of the target cannot be formed using a single set of range-only data [6].

C. TWO-DIMENSIONAL IMAGING

For sufficient target interpretation, other information is usually needed in addition to the range profile. Such added information can be in the form of a high-resolution cross-range profile, Doppler profile, or the "triangulation" of range profiles. The Synthetic Aperture Radar (SAR) and Inverse Synthetic Aperture Radar (ISAR) are examples of two different schemes of imaging systems that form two-dimensional images of a target.

"Triangulation" of different sets of range profiles allows the extension of the radar imaging concept to two dimensions. This approach permits the determination of cross-range target structure while using only HRR radar systems. It relies on collecting multiple sets of range profiles from different target orientations, processing them, and synthesizing an image.

Figures 2 and 3 illustrate this concept. Consider a set of three point targets with the radar located at the same distance from targets 2 and 3 (Figure 2). When the geometry is as in Figure 2, the return echo will only indicate two targets. This illustrates the condition where ambiguity exists when targets lie along the bands of constant range from the radar.

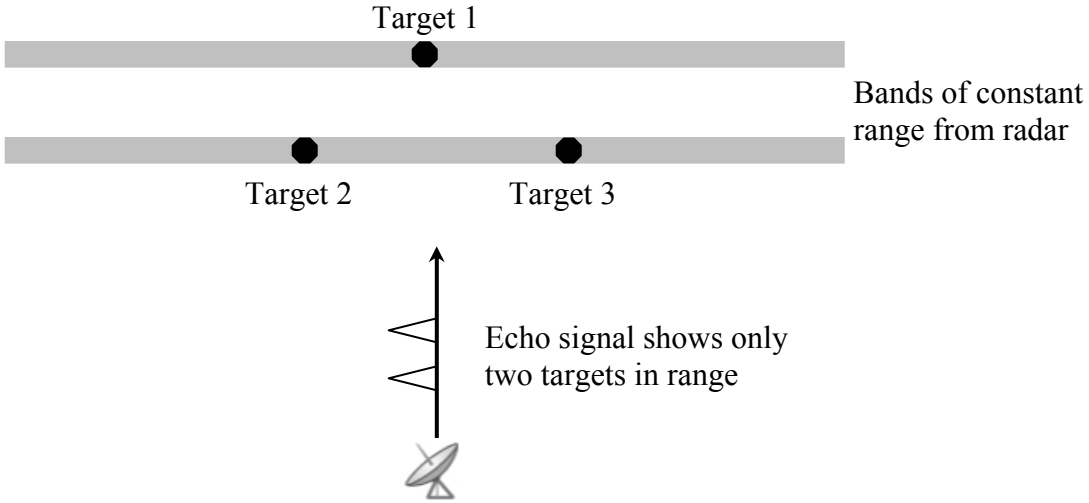

Figure 2. Ambiguity scenario from a single pulse

With multiple sets of data from different directions, triangulation will allow for gradual buildup of the relative positions of the three targets (Figure 3). The range profiles are swept in the cross-range direction to form bands of constant range from the radar, which represent the possible locations of the target scatterer. These bands are then superimposed and the crossing points are used to determine the scattering center locations. With correct correlation methods, a target image built up of points where the swept lines intersect can be obtained.

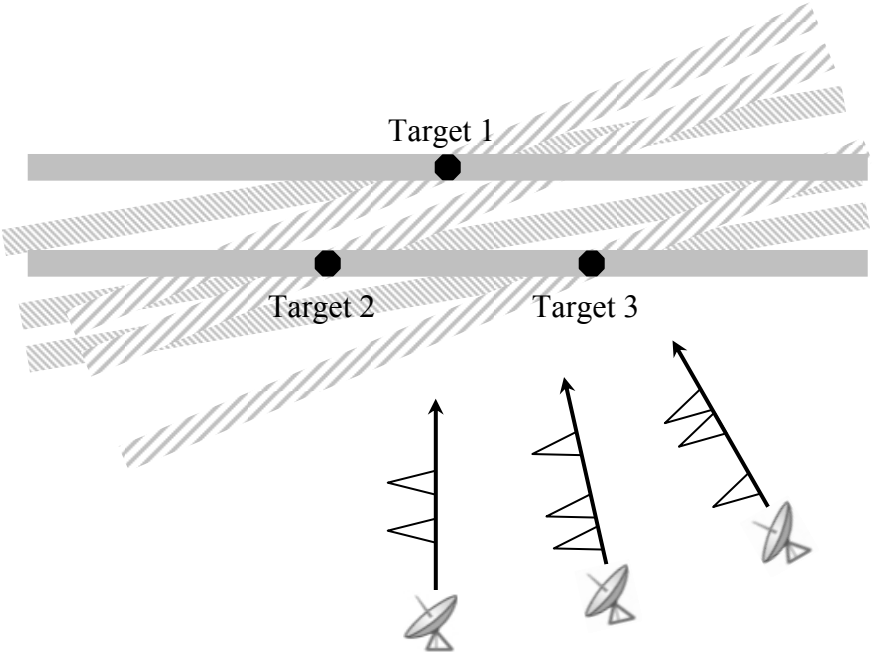

Figure 3. Cross-range information obtained from range profiles

In essence, two different schemes are used to collect target data from different target aspects to obtain cross-range information. The radar can move around the target while it remains fixed; or the target can rotate while the radar stares at it over time. In the former case, the radar is described as collecting data over a synthetic aperture, and thus, termed Synthetic Aperture Radar (SAR). In the latter case, the radar is described as an Inverse Synthetic Aperture Radar (ISAR). Mathematically, the basics for image formation are fundamentally the same for both schemes. Notwithstanding, the details of data processing, such as correcting for departures from ideal target behavior, are different in the two settings.

D. HIGH DOPPLER RESOLUTION (HDR) IMAGING

The concept of utilizing high Doppler resolution inputs to synthesize a target image can be illustrated by drawing an analogy from HRR imaging.

In HRR imaging, the image is developed by a correlation of range profiles taken at different locations. Each "line" of the range profile is an iso-range line at a specific time since the radar pulse takes a finite amount of time to reflect off a scatterer and return to the receiver.

In HDR, another set of "lines," the iso-Doppler, which are lines of constant Doppler shift at a specific frequency, is used to build the image. For a target rotating about its center, the local velocity of a scatterer will depend on its radial distance from the center. The return signal at a given Doppler shift is a superposition of all the returns due to scatterers with the same closing velocity lying along the iso-Doppler hyperbola. Conceptually, the iso-range lines and iso-Doppler lines can be considered as taking "slices" of the image, with the difference between the two being the "slices" are orthogonal to each other, as illustrated in Figure 4 [2].

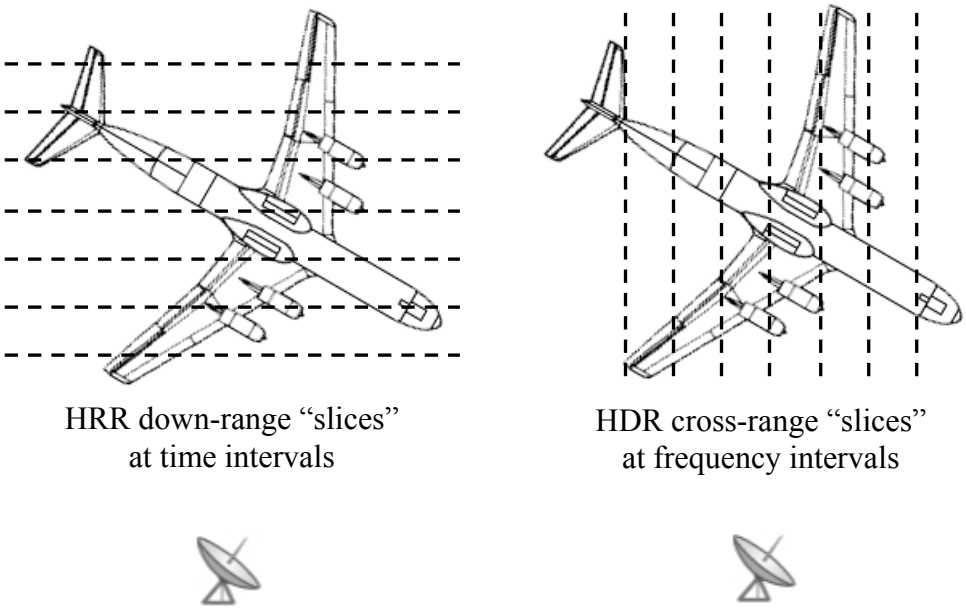

Figure 4. Orthogonal "slices" of the target between using HRR and HDR (After [2])

Similarly, ambiguities due to multiple scatterers along an iso-Doppler can be resolved by acquiring multiple Doppler profiles from different aspect angles. However, it should be noted that the HDR cross-range slices only works for rotating targets.

In HRR imaging, each range profile has high resolution in the down-range direction and the correlation of the profiles for different aspect angles will provide the cross-range resolution to build a two-dimensional image. Conversely, in HDR imaging, each Doppler profile will have high resolution in the cross-range direction and the correlation process will provide the down-range resolution.

III. INVERSE PROBLEMS IN RADAR IMAGING

A. GENERAL FORMULATION OF THE IMAGING PROBLEM

A general formulation of the imaging problem can be achieved by considering a space-invariant imaging system represented by the operator *S*, with input image *f(x)* and output image *g(x)*. They are related by Equation (3.1) and the model is illustrated schematically in Figure 5. Since the system *S* is known, a real non-negative image *g(x)* with values in a given domain $x \in \Re$, is generated at the output of the system.

$$g = Sf \tag{3.1}$$

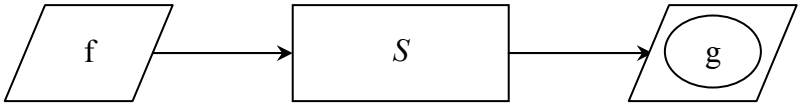

Figure 5. Image formation model

The image synthesis problem first determines if an image $f \in \Im$ (that satisfies the given constraints represented by the set $\Im$) exist such that the system output *Sf(x) = g(x)* for all $x \in \Re$ [7]. If such an image does exist, then the next step is to determine *f*. On the other hand, if the image does not exist, then the approach is to determine an approximate input image *f* that produces an output *g = Sf* according to some criterion. One possible optimization criterion for finding an approximate solution is to minimize a norm

$$\|Sf - g\| = \min$$

The solution to this general formulation will "define" the solution of inverse problems.

B. INVERSE PROBLEMS

J.B. Keller formulated the following general definition [8] of inverse problems, which is often cited in literature:

> We call two problems inverses of one another if the formulation of each involves all or part of the solution of the other. Often, for historical reasons, one of the two problems has been studied extensively for some time, while the other is newer and not so well understood. In such cases, the former problem is called the direct problem, while the latter is called the inverse problem.

A *direct problem* can be thought of as one oriented towards a cause and effect sequence, while the corresponding *inverse problem* is linked to the reversal of this cause and effect sequence and comprises determining the unknown causes of known consequences. In radar imaging, the direct problem is the mapping from the target to the quantities that can be measured by the radar.

Consequently, the inverse problem is the problem of finding the original target given the data and knowledge of the direct problem. This mapping is called the target image. However, this problem is ill-posed due to the loss of information intrinsic to the solution of the direct problem. Therefore, if an image corresponds to two distinct objects, then the solution of the inverse problem is not unique. Further, if there are two neighboring images such that the corresponding objects are very distant, then the solution of the inverse problem does not depend continuously on the data.

The accepted approach for solving inverse problems which are ill-posed is to search for approximate solutions satisfying additional constraints based on the physics of the problem [12]. This set of approximate solutions corresponding to the same data function is the set of objects with images close to the measured one.

C. WELL-POSED AND ILL-POSED PROBLEMS

The mathematical term for well-posed problems arose from a classical concept defined by Hadamard. He believed that such problems are considered *well-posed* if they satisfy the following three conditions [10]:

1. the solution is unique
2. the solution exists for any data
3. the solution depends continuously on the data and parameters

If one of the three conditions above is not satisfied, the problem is said to be *ill-posed*. Hence, an ill-posed problem is one whose solution is not unique and/or does not exist for any data and/or does not depend continuously on the data.

The third condition is motivated by the fact that the mere process of measuring data involves small errors. If the problem is well-posed, the error propagation is controlled by the condition number. Consider the solution of a linear system of algebraic equations

$$\boldsymbol{A}x = \boldsymbol{m} \tag{3.2}$$

where $\boldsymbol{m}$ is the measured data, x is the signal and $\boldsymbol{A}$ is an operator that describes the nature of the measurement system. In the case of a unique solution, if there are n variables, then there must be n independent equations in order to obtain a solution. By conditions 1 and 2, the inverse of $\boldsymbol{A}$ exists. By thinking of Δm as being the small error in the measured data and Δx as being the resulting error in x such that

$$\boldsymbol{A}(x + \Delta x) = \boldsymbol{m} + \Delta \boldsymbol{m}$$

Consequently, this uncertainty Δx complies with

$$\frac{\|\Delta x\|}{\|x\|} \leq cond(A)\frac{\|\Delta \boldsymbol{m}\|}{\|\boldsymbol{m}\|}$$

where $\|\Delta \boldsymbol{m}\| / \|\boldsymbol{m}\|$ is the relative change in measurement and $\|\Delta x\| / \|x\|$ is the relative error caused by this change [11].

The condition number is a relative error magnification factor and the quantity that controls error propagation from data to solution. It is defined as

$$cond(\boldsymbol{A}) = \|\boldsymbol{A}\|\|\boldsymbol{A}^{-1}\|$$

where the common norm of Euclidean distance is adopted for $\|\boldsymbol{A}\|$ such that

$$\|\boldsymbol{A}\| = \left(\sum_{i=1}^{m}\sum_{j=1}^{n} |a_{ij}|^2 \right)^{\frac{1}{2}}$$

It should be noted that the computation of the matrix norm corresponding to the l_2-norm criterion involves the singular value decomposition (SVD). If the condition number of $\boldsymbol{A}$ is not large, then the problem is considered to be *well-conditioned*. The solution to the problem will be stable relative to small variations of data. This requirement of stability is essential for meaningful problems in approximation methods. On the other hand, if the condition number is large, then the problem is deemed *ill-conditioned*. The ill-conditioned situation is somewhat similar to the ill-posed condition. An ill-posed problem can be thought of as one where an inverse does not exist because $\boldsymbol{m} + \Delta\boldsymbol{m}$ is outside the range of $\boldsymbol{A}$.

In general, most inverse problems are ill-posed. In the case of a bandlimited system, the solution of the inverse problem is not unique and the first condition required for well-posedness is not satisfied. This is because the imaging system does not transmit information about the target at frequencies outside the band of the instrument.

Straightforward solutions of ill-posed problems can result in non-physical answers. It is interesting to note that a more refined operator $\boldsymbol{A}$ may work against obtaining a more reliable solution. When discretizing an ill-posed problem, the condition number of the corresponding discrete problem can be very large. It is the case that, when the discretization of the ill-posed problem gets finer, the condition number of the corresponding discrete problem becomes larger [9]. For this reason, the discretization of equations must be done carefully and techniques must be introduced to construct stable solutions.

D. METHOD OF LEAST SQUARES

An overdetermined system is one that comprises more equations than unknowns. Overdetermined systems of simultaneous linear equations are often encountered in various kinds of curve fitting to experimental data. The method of least squares is frequently used to solve such systems of equations in an approximate sense. During the process of measuring data, errors or inaccuracies will be manifested in the measurement. Hence, instead of solving the equations accurately, the minimization of the sum of

squares of the residuals is sought. The result is a curve fit to a set of data points such that the sum of squares of the range between the data point and its corresponding curve is minimized.

If appropriate probabilistic assumptions about underlying error distributions are made, the least squares approach becomes what is known as the *maximum-likelihood* estimate of the parameters. This least squares criterion (l_2 -norm criterion) is widely used for the resolution of inverse problems due to its simplicity. It should be noted that at times, it is applied even if its basic underlying hypothesis (Gaussian uncertainties) is not always satisfied [13].

In the curve fitting model, let *t* be the independent variable and let *m(t)* denote the unknown function of *t* to be approximated. If there are *k* observations, then the values of *m* measured at specified points of *t* are

$$m_i = m(t_i), \qquad i = 1, 2, ..., k$$

The function *m(t)* is then modeled by a linear combination of *n* basis functions

$$m(t) \approx x_1\phi_1(t) + ... + x_n\phi_n(t)$$

The design matrix A is a rectangular matrix of order *k* by *n* with elements

$$a_{ij} = \phi_j(t_i)$$

In matrix-vector notation, the model is

$$\boldsymbol{m} \approx \boldsymbol{A}x$$

There are many models available for the curve fitting solution. Some common models include the straight line, polynomials, rational functions, exponentials, log-linear and Gaussian. This thesis will focus on applying the polynomial model for the least squares application. The model used is a cubic polynomial of the form

$$m(t) \approx x_1 + x_2 t + x_3 t^2 + x_4 t^3$$

The residuals are the differences between the measurements and the model:

$$
\begin{aligned}
r_i &= m_i - \sum_{j=1}^{n} x_j \phi_j(t_i) \qquad i = 1, 2, ..., k \\
&= m_i - m(t) \\
&= m_i - \left(x_1 + x_2 t + x_3 t^2 + x_4 t^3 \right)
\end{aligned}
$$

By the method of least squares, the objective is to minimize the sum of squares of the residuals:

$$
\|r\|^2 = \sum_{i=1}^{k} r_i^2
$$

$$
\Rightarrow \|r\|^2 = \sum_{i=1}^{k} \left[m_i - \left(x_1 + x_2 t + x_3 t^2 + x_4 t^3 \right) \right]^2 \tag{3.3}
$$

E. CORRELATION RECEPTION

In radar processing, correlation reception is an important technique that allows the accurate separation of the desired signal from the unwanted noise. It involves the comparison of the received signal with reference signals of the form

$$
s_{scatt}(t') = \rho s_{scatt}(t' - t) e^{iv(t'-t)} \tag{3.4}
$$

where $s_{scatt}(t')$ is the radar signal associated with the field reflected from an object at range t and radial velocity v and ρ is a signal strength scale factor [14]. This comparison is performed coherently such that the phase of the transmission signal is preserved in the reference signal. The correlation receiver can be considered as a type of matched filter receiver.

The original radar signal processing problem involves optimal detection in additive noise so that the received signal is of the form

$$
s_{rec}(t) = s_{scatt}(t) + n(t) \tag{3.5}
$$

where $n(t)$ is a random noise process and $s_{rec}(t)$ is the received signal measured by the radar. The objective is to determine $s_{scatt}(t)$ from the random measurements of $s_{rec}(t)$. Estimation is usually accomplished through maximum likelihood processing whereby $s_{rec}(t)$ is compared to some idealized signals generated using a signal model. The

maximum likelihood estimate for $s_{scatt}(t)$ is one which maximizes the probability $p_{s_r|s_{sc}}$, which is the conditional probability density function of the measured signal for a specific scattered field $s_{scatt}(t)$ [6].

$$s_{scatt,ML} = \arg \max_{\text{u} \in \text{ model space}} p_{s_r|s_{sc}}(u)$$

Consequently, it can be shown that correlation receivers attempt to determine the time shift, τ, and frequency shift, υ, which maximizes the real part of the correlation integral

$$\eta(\upsilon,\tau) = \int_{-\infty}^{\infty} s_{rec}(t') s_{inc}^{*}(t'-\tau) e^{-i\upsilon(t'-\tau)} dt' \tag{3.6}$$

In radar operations, the natural model is based on the scattering interaction between the interrogating field and target. If $s_{inc}(t)$ is the incident pulse transmitted by the radar, then the linear radar scattering model is derived from the superposition of Equation (3.4).

$$s_{scatt}(t) = \int\int_{-\infty}^{\infty} \rho(\upsilon,\tau) \text{s}_{inc}(t-\tau) e^{i\upsilon(t-\tau)} d\tau d\upsilon \tag{3.7}$$

Now, this model is substituted into Equation (3.5) and then into the correlation integral of Equation (3.6).

$$\eta(\upsilon,\tau) = \int\int\int_{-\infty}^{\infty} \rho(\upsilon',\tau') \text{s}_{inc}(t'-\tau) s_{inc}^{*}(t'-\tau') e^{i\upsilon'(t'-\tau)} e^{-i\upsilon(t'-\tau')} dt' d\tau' d\upsilon'$$

$$+ \text{ correlation noise term} \tag{3.8}$$

The correlation noise term is considered small and can thus be ignored. Thereafter, Equation (3.8) can be rearranged to

$$\eta(\upsilon,\tau) = \int\int_{-\infty}^{\infty} \rho(\upsilon',\tau') \chi(\upsilon-\upsilon',\tau-\tau') e^{i\frac{1}{2}(\upsilon+\upsilon')(\tau-\tau')} d\tau' d\upsilon' \tag{3.9}$$

where

$$\chi(\upsilon,\tau) = \int_{-\infty}^{\infty} s_{inc}(t'-\frac{1}{2}\tau)\, s_{inc}^{*}(t'+\frac{1}{2}\tau) e^{i\upsilon t'} dt' \tag{3.10}$$

Equation (3.9) is the standard radar data model and expresses the output of the correlation receiver as the convolution of ρ and χ. The function $\chi(\upsilon,\tau)$ defined by Equation (3.10) is the ambiguity function.

F. AMBIGUITY FUNCTION

The accuracy with which the target position and radial velocity can be estimated from the radar data is determined by the ambiguity function. In radar systems, waveforms are selected to optimize the requirements of detection, measurement accuracy, resolution, and ambiguity and clutter rejection. Ambiguity function plots are scrutinized for a qualitative determination of the suitability of different waveforms in meeting the above requirements [4]. In practice, the ambiguity function is plotted as a function of time delay and Doppler shift. In radar imaging, the ambiguity function can be thought of as the imaging kernel.

1. Ambiguity Function for HRR Signal

In HRR imaging, the system can be represented by an impulse radar transmitting a very short pulse in the form of a Dirac delta function

$$s_{inc}(t) = \delta(t)$$

The ambiguity function becomes

$$\begin{aligned}\chi(\upsilon,\tau) &= \int_{-\infty}^{\infty} s_{inc}(t'-\frac{1}{2}\tau)\, s_{inc}^{*}(t'+\frac{1}{2}\tau)e^{i\upsilon t'}dt' \\ &= \int_{-\infty}^{\infty} \delta(t'-\frac{\tau}{2})\delta(t'+\frac{\tau}{2})e^{i\upsilon t'}dt'\end{aligned}$$

$$\therefore \chi(\upsilon,\tau) = \delta(\tau)e^{i\upsilon\frac{\tau}{2}}$$

The data collected from such a radar is independent of frequency shift and is known as the down-range profile. In reality, a Dirac delta function does not exist physically, hence, the waveform used is usually an approximation of an impulse.

2. Ambiguity Function for HDR Signal

In HDR imaging, the system can be represented by a continuous wave radar transmitting a single tone signal in the form

$$s_{inc}(t) = e^{-i\omega t}$$

The ambiguity function then becomes

$$\begin{aligned}\chi(\upsilon,\tau) &= \int_{-\infty}^{\infty} s_{inc}(t'-\frac{1}{2}\tau)\, s_{inc}^{*}(t'+\frac{1}{2}\tau)e^{i\upsilon t'}dt' \\ &= \int_{-\infty}^{\infty} e^{-i\omega(t'-\frac{\tau}{2})} e^{i\omega(t'+\frac{\tau}{2})} e^{i\upsilon t'}dt' \\ &= e^{i\omega\tau}\int_{-\infty}^{\infty} e^{i\upsilon t'}dt'\end{aligned}$$

$$\therefore \chi(\upsilon,\tau) = \delta(\upsilon)e^{i\omega\tau} \tag{3.11}$$

It can be concluded that the data collected is independent of down-range delay. Consequently, such radar data can be used to determine the distribution of down-range velocity accurately, but will offer no information about target position.

3. Bistatic Ambiguity Function

For a monostatic radar, the use of delay and Doppler shift as the arguments of the ambiguity function is sufficient due to the linear relationship between target range and range rate. Thus, the delay and Doppler shift pair, or the range and range rate pair, may be used interchangeably in the ambiguity function.

In the case of a bistatic or multistatic radar, the situation is more complicated. Since the transmitter and receiver are not at the same site, the relationship between Doppler shift and target velocity, and between time delay and range, are highly non-linear. The shape of the ambiguity function is a strong function of the geometry between the transmitter, receiver and target, as well as waveform properties [15]. Hence, the representation of the ambiguity function for a bistatic radar in terms of delay and Doppler shift is not meaningful and may even lead to incorrect conclusions.

It has been proposed that the ambiguity function for bistatic radar be written as:

$$\chi(R_{RH}, R_{Ra}, V_H, V_a, \theta_R, L) =$$
$$\left| \int_{-\infty}^{\infty} s(t - \tau_a(R_{Ra}, \theta_R, L) \cdot s^*(t - \tau_H(R_{RH}, \theta_R, L) \cdot e^{\left[-i(\omega_{DH}(R_{RH}, V_H, \theta_R, L) - \omega_{Da}(R_{Ra}, V_a, \theta_R, L))t\right]} dt \right|^2 \quad (3.12)$$

where R_{RH} and R_{Ra} are the hypothesized and actual ranges from the receiver to the target; V_H and V_a are the hypothesized and actual radial velocities of the target relative to the receiver; ω_{DH} and ω_{Da} are the hypothesized and actual Doppler shift; θ_R is the bearing of the target with respect to the receiver; and L is the baseline length between the transmitter and receiver [16]. Equation (3.12) assumes the reference point of the bistatic geometry to be the receiver. The main difference between Equations (3.12) and (3.10) is that the geometrical disposition of the transmitter, receiver, and target are taken into account.

IV. BISTATIC AND MULTSTATIC RADAR THEORY

A. BACKGROUND

In monostatic radar systems, increased information is frequently associated with increased bandwidth. With the increased bandwidth, high range resolution is obtainable and frequency diversity offers one such approach to obtain additional information about targets. On the other hand, in a multistatic radar system, *geometric diversity* [17] in the disposition of transmitting and receiving stations allows additional target information to be obtained. With suitable signal processing, the additional information obtained can translate into improved target detection. Additionally, geometric diversity offers the potential for increased resolution and it is a dual to frequency diversity in classical monostatic radar systems. Hence, improved target position accuracy and image resolution can be expected in a multistatic radar system.

The image resolution for the monostatic synthetic aperture radar (SAR) can be drawn from tomography/Fourier space or radar range/Doppler principles. In the case of multistatic SAR, the resolution result is understood using the tomography/Fourier space principles. As an example, an ultra wideband monostatic SAR with a 50% bandwidth will have a range resolution of λ and a pixel area of λ^2. A Multistatic SAR system will have a range resolution of $\lambda/3$ and a pixel area of $\lambda^2/9$ [18]. This translates to a 9.5 dB improvement over monostatic. A similar performance gain can be expected from a multistatic ISAR system.

Since the bistatic radar is the building block for the multistatic radar system, the fundamental theory for bistatic radar operation will first be discussed. These will include the coordinate system, the determination of target location and Doppler information and resolution. Thereafter, the extension of the bistatic radar to the multistatic radar system, its advantages and drawbacks, and implementation requirements will be examined.

B. DEFINITION OF BISTATIC RADAR

As defined by the IEEE Standard 686-1997 [1], the bistatic radar is a radar using antennas for transmission and reception at sufficiently different locations that the angles or ranges from those locations to the target are significantly different. Bistatic radar is deemed to have significant advantages against stealthy targets due to the relatively larger amount of forward scattering. Furthermore, the operation of the bistatic radar receiver is considered covert, as its location cannot be determined easily by merely observing the radar's emissions.

Figure 6 illustrates the setup of a bistatic radar, with a transmitter *Tx* and receiver *Rx* situated at two different locations, separated by a baseline distance *L*. The bistatic angle β is the angle between the transmitter and receiver with the vertex at the target.

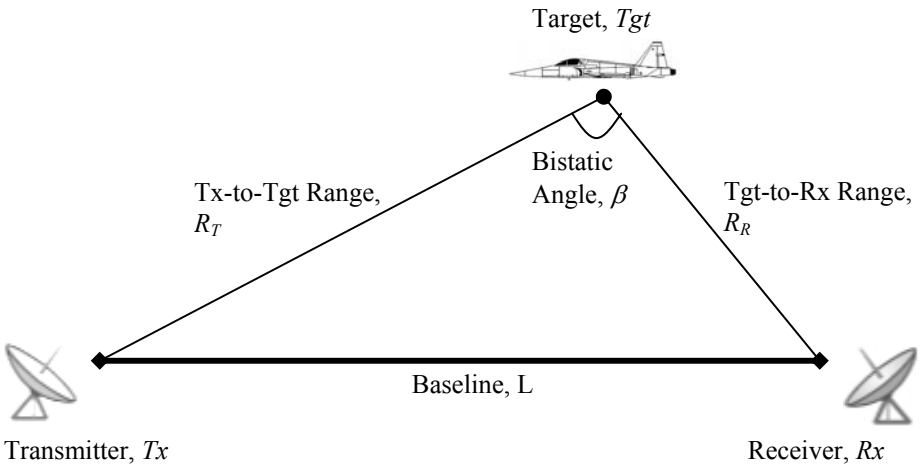

Figure 6. Bistatic radar

C. COORDINATE SYSTEM

This thesis will adopt a two-dimensional, North-referenced coordinate system for derivation and discussion. Figure 7 depicts the coordinate system and the parameters characterizing bistatic radar operation. The plane containing the transmitter, receiver and target is defined as the bistatic plane and the bistatic triangle lies in this plane. The angles, ϕ_T and ϕ_R, are the respective target bearings for the transmitter and receiver. They are taken to be positive when measured clockwise from North. The angle $\beta/2$ is known as the bistatic bisector angle. It should be noted that $\beta = \phi_T - \phi_R$.

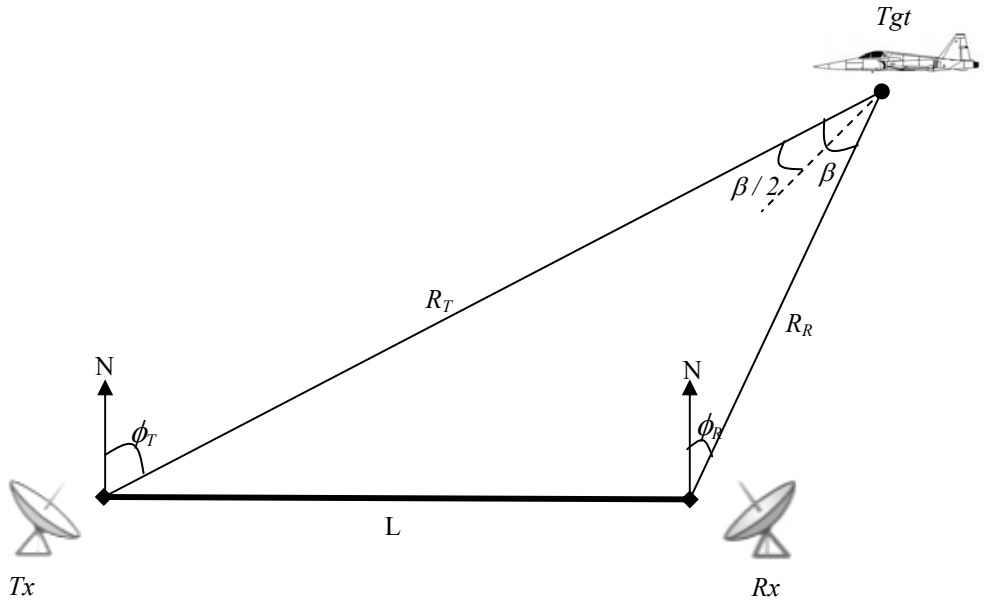

Figure 7. Bistatic radar (North referenced) coordinate system

D. TARGET LOCATION

The target's position relative to the receiving station can be determined if R_R and ϕ_R can be obtained. However, the receiver-to-target range, R_R, cannot be measured directly as a bistatic radar usually measures target range as the range sum $R_T + R_R$. It can be calculated by solving the bistatic triangle of Figure 7. From the cosine rule, R_T and R_R are calculated as follows:

$$R_T^2 = R_R^2 + L^2 - 2R_R L\cos\left(\frac{\pi}{2} + \phi_R\right)$$

$$R_R^2 + 2R_R L\sin(\phi_R) = R_T^2 - L^2$$

$$2R_R^2 + 2R_R L\sin(\phi_R) + 2R_T R_R = (R_T + R_R)^2 - L^2$$

$$\Rightarrow \qquad R_R = \frac{(R_T + R_R)^2 - L^2}{2\left[(R_T + R_R) + L\sin(\phi_R)\right]} \tag{4.1}$$

From equation (4.1), R_R can be determined once the range sum $R_T + R_R$ is obtained and ϕ_R is known. Thereafter, R_T can be expressed as follows:

$$R_T = \sqrt{R_R^2 + L^2 - 2R_R L\sin(\phi_R)} \tag{4.2}$$

Alternatively, R_T can also be expressed in terms of the range sum $R_T + R_R$ and ϕ_T by making use of the cosine rule.

$$R_T = \frac{\left(R_T + R_R\right)^2 - L^2}{2\left[\left(R_T + R_R\right) - L\sin\left(\phi_T\right)\right]} \tag{4.3}$$

The range sum $R_T + R_R$ can be determined by two methods, namely direct and indirect. In the *direct* method, the receiver measures the time interval ΔT_D, between reception of the transmitted pulse and reception of the target echo. Adequate line of sight between transmitter and receiver is required. The range sum is then calculated as

$$\left(R_T + R_R\right) = c\Delta T_D + L \tag{4.4}$$

In the *indirect* method, synchronized stable clocks are used by the receiver and a dedicated transmitter. Line of sight between transmitter and receiver is not required for this measurement. The receiver measures the time interval ΔT_I between transmission of the pulse and reception of the target echo. The range sum is then calculated as

$$\left(R_T + R_R\right) = c\Delta T_I \tag{4.5}$$

For this thesis, the *direct* method of time interval measurement is adopted.

Additionally, from the sine rule, the following relationships are obtained:

$$\frac{\sin(\beta)}{L} = \frac{\sin\left(\frac{\pi}{2} + \phi_R\right)}{R_T} = \frac{\sin\left(\frac{\pi}{2} - \phi_T\right)}{R_R} \tag{4.6}$$

$$\Rightarrow \qquad \frac{R_R}{R_T} = \frac{\cos(\phi_T)}{\cos(\phi_R)} \tag{4.7}$$

$$\frac{R_R}{L} = \frac{\cos(\phi_T)}{\sin(\beta)} \tag{4.8}$$

$$\frac{R_T}{L} = \frac{\cos(\phi_R)}{\sin(\beta)} \tag{4.9}$$

E. TARGET DOPPLER

The bistatic Doppler shift, f_B, is defined as the time rate of change of the total path length of the scattered signal, normalized by the wavelength λ. Since the total path length is the range sum of $R_T + R_R$, the target Doppler shift is as follows.

$$f_B = \frac{1}{\lambda}\left(\frac{d}{dt}\left(R_T + R_R\right)\right) = \frac{1}{\lambda}\left(\frac{dR_T}{dt} + \frac{dR_R}{dt}\right) \tag{4.10}$$

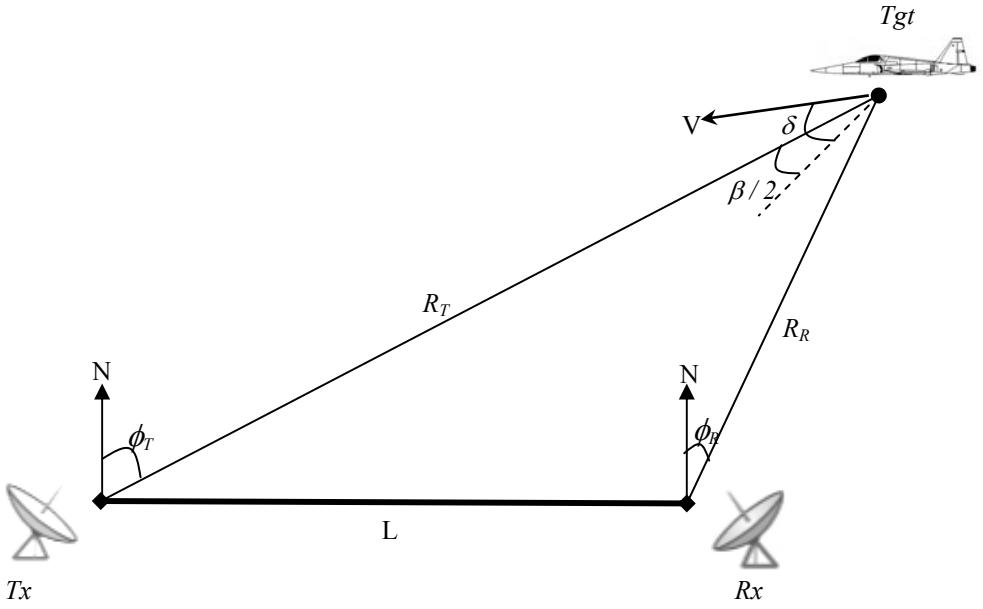

Figure 8. Bistatic Doppler geometry

In the case when the transmitter and receiver are stationary while the target is moving (see Figure 8), the target's bistatic Doppler shift at the receiver station can be expressed as a function of the aspect angle referenced to the bistatic bisector, δ. The corresponding Doppler shift is derived as follows:

$$\frac{dR_T}{dt} = V\cos\left(\delta - \frac{\beta}{2}\right) \tag{4.11}$$

$$\frac{dR_R}{dt} = V\cos\left(\delta + \frac{\beta}{2}\right) \tag{4.12}$$

$$f_B = \frac{V}{\lambda}\left[\cos\left(\delta - \frac{\beta}{2}\right) + \cos\left(\delta + \frac{\beta}{2}\right)\right]$$

$$\Rightarrow f_B = \frac{2V}{\lambda}\cos(\delta)\cos\left(\frac{\beta}{2}\right) \tag{4.13}$$

The properties of Equation (4.13) are presented in Table 1.

Condition	Property
All β	Magnitude of the bistatic target Doppler shift is never greater than that of the monostatic target Doppler shift, when the monostatic radar is located on the bistatic bisector.
All β $-90° < \delta < +90°$	Bistatic target Doppler shift is positive.
All β $\delta = \pm 90°$	Bistatic Doppler shift is zero.
All $\beta < 180°$ $\delta = 0°$ or $180°$	Target's velocity is collinear with bistatic bisector. Magnitude of bistatic target Doppler shift is maximum.
$\beta = 180°$	Target is on the baseline, characterized by large forward scatter. Radar can only detect presence of a target, the range is indeterminate due to eclipsing of the direct pulse by the scattered pulse.

Table 1. Properties of bistatic Doppler shift under various conditions (From [22])

F. DOPPLER RESOLUTION

For both monostatic and bistatic radars, the Doppler resolution depends on the amount of Doppler separation between two target echoes at the receiver, f_{B1} and f_{B2}. It is accepted to be $1/T$, where T is the receiver's coherent processing interval [20]. Hence, the requirement for Doppler resolution is

$$f_{B1} - f_{B2} = \frac{1}{T} \tag{4.14}$$

In the bistatic case, an example of the geometry for two targets is as shown in Figure 9. These targets are assumed to be collocated; consequently, they share a common bistatic bisector. The corresponding bistatic target Doppler shifts are

$$f_{B1} = \frac{2V_1}{\lambda}\cos(\delta_1)\cos\left(\frac{\beta}{2}\right)$$

$$f_{B2} = \frac{2V_2}{\lambda}\cos(\delta_2)\cos\left(\frac{\beta}{2}\right)$$

Combining these equations, the bistatic Doppler resolution can be obtained from the difference between the two target velocity vectors, projected onto the bistatic bisector.

$$\Delta V = V_1\cos(\delta_1) - V_2\cos(\delta_2)$$

$$\Rightarrow \Delta V = \frac{\lambda}{2\mathrm{T}\cos\left(\frac{\beta}{2}\right)} \tag{4.15}$$

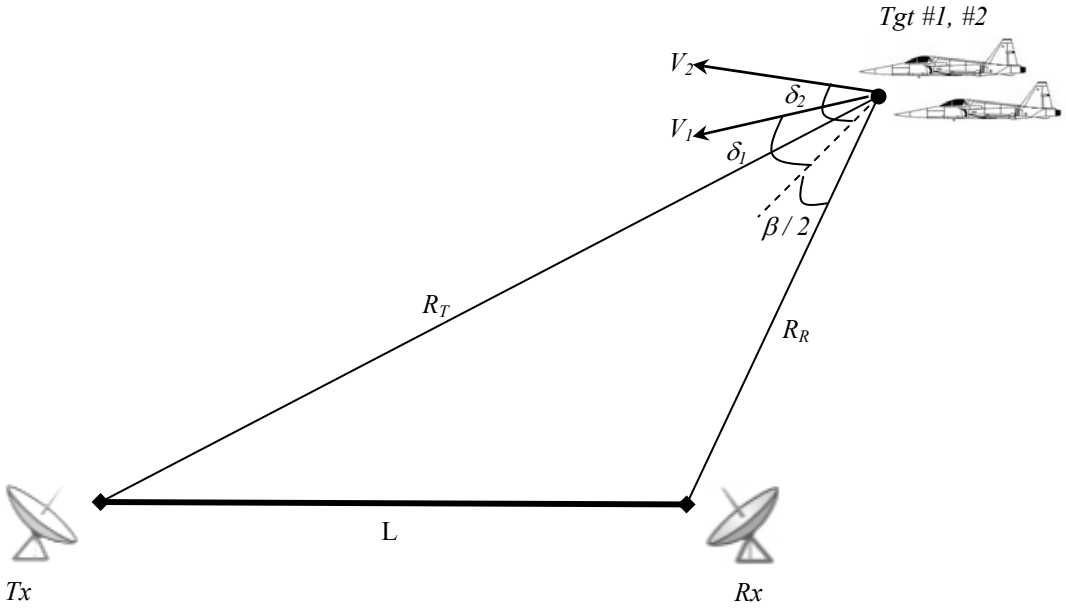

Figure 9. Bistatic Doppler resolution (for 2 collocated targets)

G. DEFINITION OF MULTISTATIC RADAR

The IEEE Standard 686-1997 [1] has defined the multistatic radar as a radar system having two or more transmitting or receiving antennas with all antennas separated by large distances when compared to the antenna sizes. It comprises at least three components - one transmitter and two receivers, or multiple receivers and multiple transmitters. It is an extension of the bistatic radar system, with one or more receivers

processing returns from one or more geographically separated transmitters. Examples of such radar systems include the Air Force Space Surveillance System and the Silent Sentry System. Figure 10 depicts an illustration of a multistatic radar set up.

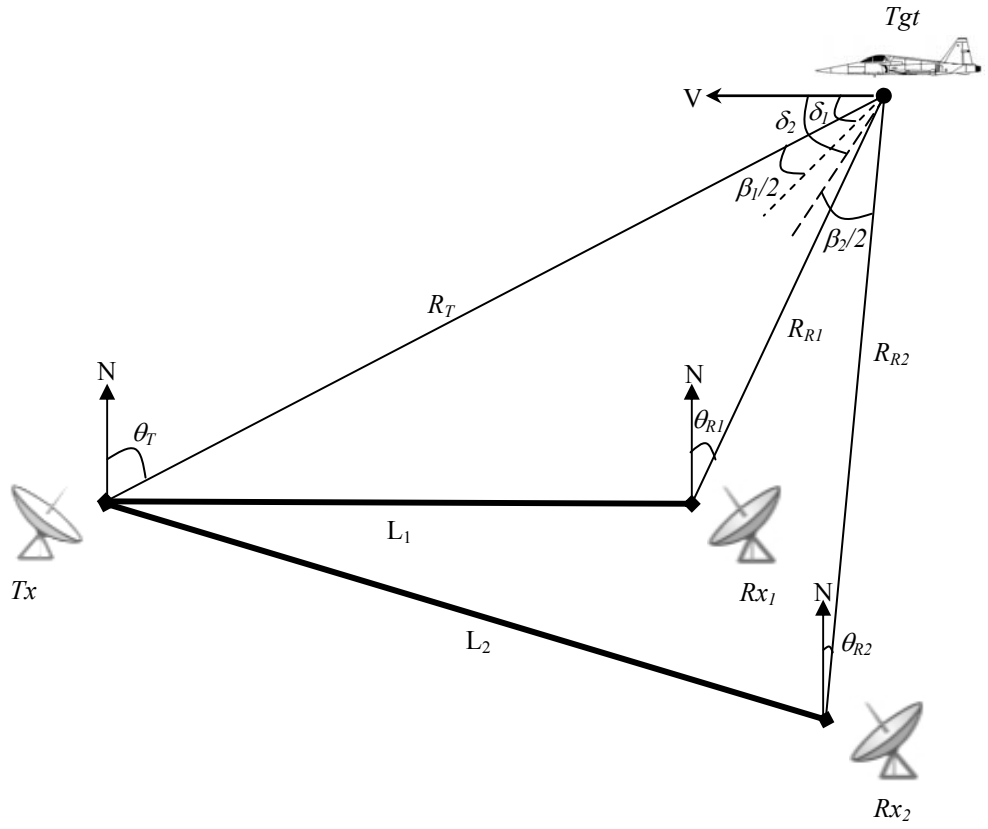

Figure 10. Sample Multistatic radar configuration (1 transmitter & 2 receivers)

H. MAIN ADVANTAGES

Due to information fusion from several spatially separated receiving stations, the multistatic radar has significant advantages over a basic monostatic radar. Some of these advantages include accurate target position estimates, Doppler estimation, coordinate measurement, increased resolution, power advantages, flexible configuration, and improved clutter rejection [21].

1. Accurate Position Estimate of Targets

In a conventional monostatic radar, target position determination is more accurate in down-range than in cross-range direction. The multistatic radar allows the estimation of the target coordinates through range-sum measurements relative to the spatially separated transmitting and receiving stations.

The track update rate may usually be higher in a multistatic radar than in a monostatic radar, and consequently, higher tracking accuracy can be achieved.

2. Doppler Estimation of Target Velocity and Acceleration

Doppler frequency shifts measured at the various receiving stations allow the estimation of the target's velocity vector. With Doppler information, trajectory information of a target can be estimated with accuracy in a short time interval. The use of Doppler frequency shifts for velocity and acceleration estimates improve tracking accuracy and general quality of the tracking process.

3. Measurement of Three Dimensional Coordinates and Velocity

Monostatic or bistatic radars can only determine the signals' Directions Of Arrival (DOA) based on the bearings of the radiation sources. Multistatic radars can obtain the three-dimensional coordinates and their derivatives by triangulation, hyperbolic methods, or their combination. *Triangulation* determines the position based on the intersection of DOA from various receiving stations. The *hyperbolic method* determines the position based on the intersection of hyperboloids of revolution, which have their foci at receiving stations. A fixed Time Difference Of Arrival (TDOA) at a pair of stations determines a hyperboloid of revolution on which surface the target must lie. This TDOA is estimated by the signal delay in one station, which is necessary to maximize the mutual correlation of signals received by the two stations [21].

The measurement of Doppler frequency shifts of the mutual correlation function of signals received by a pair of receiving stations from a moving target allows the multistatic radar to estimate the radial velocity relative to these stations. A multistatic

radar system comprising four or more stations will be able to obtain all three components of the target velocity vector by Doppler frequency shift measurements.

4. Increased "Signal Information" of Target Body

"Signal information" [21] refers to the information extracted from target echoes that concerns geometrical, physical and other features such as movement relative to target center of mass. When a target is observed by a multistatic radar system from different directions simultaneously, the total amount of signal information may be significantly more substantial than that from a monostatic radar. With the signals received by spatially separated receiving stations, the size, form and relative motion of a target can be measured with higher accuracy and in a shorter time interval. Additionally, two-dimensional and even three-dimensional radar images of the target can be obtained if the transmitting and receiving stations are spatially coherent.

5. Increased Resolution

The radar's resolution capability in measuring a target's range, bearing or velocity is related to the extent of the response of echo from a point target. High resolution information of the target may be achieved in a multistatic radar system if the signals at the receiving stations are spatially correlated. Using the hyperbolic method, these signals undergo correlation processing and two sources of mutually uncorrelated radiations, located within the main lobe of the receiving station's antenna, can be resolved by the system.

6. Power Advantages

The multitude of transmitting and receiving stations in the multistatic radar system has additional power advantages compared to monostatic radar. Each receiving station can exploit the energy transmission from all transmitting stations and enjoy significant power benefits. When the baseline distances are adequately long, scattered signal fluctuations are statistically independent at different receiving stations. Information fusion may lead to additional power gain due to fluctuation smoothing. Additionally, when stations are separated such that the angle between directions from a

target to a transmitting and a receiving station approaches 180°, the radar cross section (RCS) and the scattered signal intensity may increase significantly at the receiving stations. This increase in RCS cannot be completely reduced by stealth technologies such as body shaping and application of radar absorbent material coating. Furthermore, since the transmitter and receiver are spatially separated, receiver protection devices such as duplexer and circulator are not required. Consequently, signal power losses are reduced.

7. Configurable Coverage Area

System geometry and fusion algorithms in a multistatic radar system permit the extension of coverage area in the required direction. If the radar system is comprised of mobile transmitter and/or receiver units, the reconfiguration of coverage area can be achieved easily.

8. Improved Clutter Rejection

In a multistatic radar system, since the transmitting and receiving stations are physically separated, the intersection volume of their main beams may be much less than the main beam volume of a monostatic radar. Under certain conditions, a significant reduction in clutter intensity can result. Additionally, moving target indication (MTI) techniques perform better in a multistatic radar than a monostatic radar. When the radial velocity of a target relative to a monostatic radar is zero, MTI techniques are useless. In a multistatic radar system, a moving target cannot generally present zero radial velocity to several spatially located receiving stations. Similarly, the limitation of blind radial velocities in a monostatic radar is overcome.

I. MAIN DRAWBACKS

With the increased number of stations and components in a multistatic radar, the added complexities also impose difficulties in the implementation. Some of these drawbacks include the requirement for synchronization and mutual alignment, the need for direct line of sight between stations and targets, the need for data transmission lines, and increased processing requirements [21].

1. Synchronization, Phasing and Transmission of Reference Signals

Synchronization between the transmitting, receiving stations and control center is necessary for accurate target coordinate measurement by the hyperbolic methods. When cooperative signal reception is used in the multistatic radar system, the receivers must know the signal waveform sent out by the transmitting stations. This can be achieved by signal transmission through the data transmission lines or transmission of synchronization codes to correct frequency and signal waveform. For coherent signal processing, a common reference frequency is required at each station to couple the transmitters' and receivers' heterodyne frequencies.

2. Requirement for Direct Line of Sight between Stations and Targets

The coverage of a multistatic radar system is limited by the necessity for direct lines of sight between stations and targets. If a target is not concurrently visible to several transmitting and receiving stations, information fusion cannot be achieved. This is an important constraint, especially for ground-based multistatic radar systems in the detection of low-level targets.

3. Need for Data Transmission Lines

These data transmission lines are used for signal or data transmission from the stations to the control center, as well as command and control information transmissions. These transmission lines need to be protected against interference and direct physical attacks.

4. Increased Processing Requirement

In a multistatic radar system, the significant increase in information from a target as compared with a monostatic radar will require fast processors for processing these data in real time. Additionally, the coordinate conversion of local radar data from each receiving station into a common coordinate system and the interstation data association between measurements impose added processing needs. Furthermore, geometrical and tracking algorithms are also more complex than those applied in monostatic radars.

5. Need for Accurate Station Positioning and Mutual Alignment

The accurate fusion of target information from several spatially located stations requires the precise knowledge of the stations' positions and their alignment. Positions of stationary stations can be obtained accurately by geodetic methods. However, the determination of positions of mobile stations will require additional navigation methods such as GPS information. Errors in station positions and their misalignment will lead to systematic errors of target location determination.

J. IMPLEMENTATION REQUIREMENTS

It is important that signal synchronization and spatial coherence among transmitting and receiving stations be established.

Signal synchronization is required between the transmitting station and receiving station for range measurement [22]. Time synchronization can be accomplished by receiving the signal directly from the transmitter. This transmitting signal can be sent directly if an adequate line of sight exists between the transmitter and receiver, via land line or other communication links if such line of sight cannot be achieved. For these direct synchronization means, the implementation is relatively straightforward.

Establishing spatial coherence (amplitude and phase) between each transmitting and receiving station, and the coherent combination of signals from all receiving stations are essential for coherent multistatic radar operation [23]. For a ground-based multistatic radar system, a viable solution is the establishment of suitable data links between the elements and the central information center.

In general, a multistatic radar could be easily implemented when the positions of all transmitting and receiving stations are at fixed locations.

For the purpose of this thesis research, it is assumed that only the *synchronization signal* and *Doppler shift* information received by each receiving station are available to the multistatic radar system for processing. Thus, the challenge is to resolve the geometry and obtain accurate position and velocity details of the targets based on limited amount of available information.

THIS PAGE INTENTIONALLY LEFT BLANK

V. RADAR MODEL DESIGN

A baseline design and approach has been developed to demonstrate the concept of high resolution imaging. The initial radar model is based on the basic multistatic radar configuration presented in the preceding chapter, with additional parameters included to aid in the derivation of the required parameters. Figure 11 depicts such a framework and the corresponding parameters.

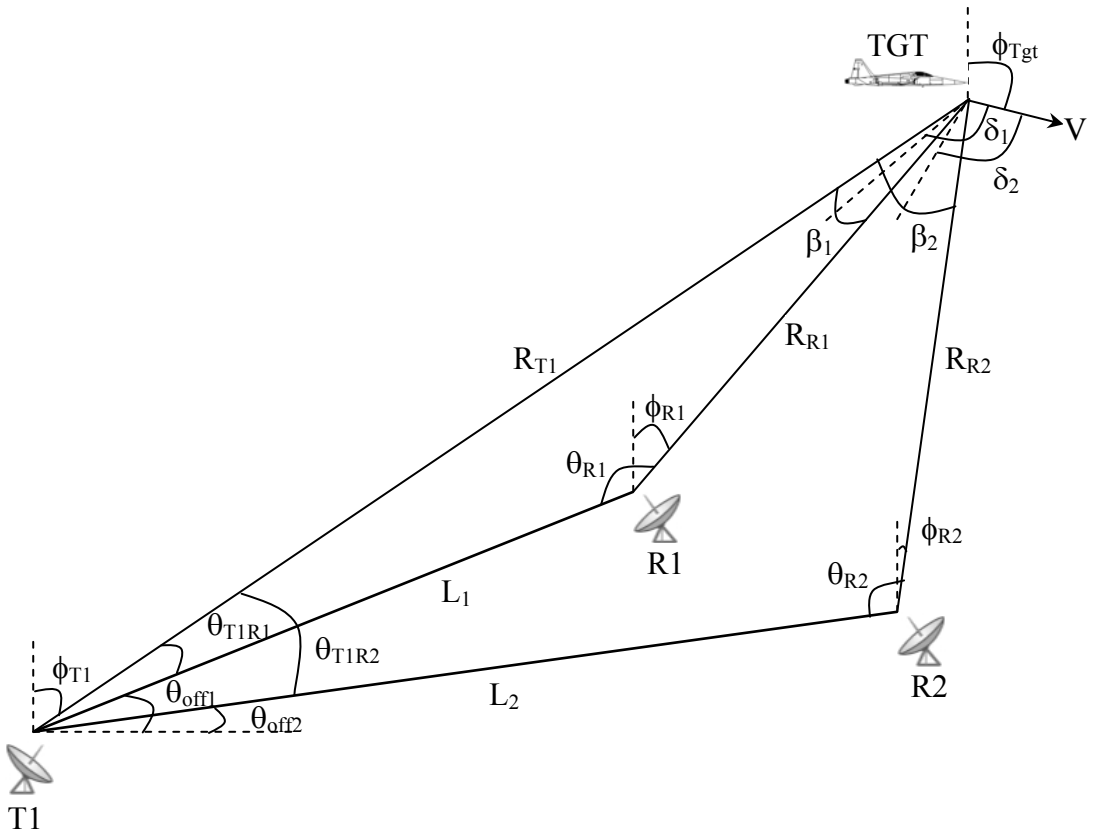

Figure 11. Framework for initial Multistatic radar model

A. ASSUMPTIONS

The radar system is assumed to use antennas with relatively low gain. Hence, the wide beam width makes it unsuitable for direct measurement of target bearing. It is believed that the implementation of such a system is feasible and the focus is on the localization of the targets and the resultant formation of the target images.

For the purpose of this thesis research, it is assumed that only the *time synchronization signal* and *Doppler shift* information received by each receiving station are available to the multistatic radar system for processing. With the time synchronization signal, the range sum, $R_T + R_R$, could be derived. The Doppler shift will result in the knowledge of the target's velocity vector.

Since the focus of this thesis is a proof of concept, it is assumed that, for ease of demonstration, the operational area of interest is a flat two-dimensional plane. After the concept has been proven, the more realistic three-dimensional space can be extended in a relatively straightforward manner.

The target is assumed to behave like a rigid body. Non-rigid bodies can be modeled by multiple targets with varying velocity vectors.

A flat earth has also been assumed to simplify the derivation and demonstration.

B. MODEL NOTATIONS

The notations used in the subsequent derivation are presented in Table 2.

Parameter	Notation	Description
Bearing	$\phi_{Tgt}, \phi_{T1}, \phi_{R1}, \phi_{R2}$	Heading using North-referenced coordinate system
Bistatic Angle	β_1, β_2	Bistatic angle for each Transmitter-Target-Receiver bistatic system
Aspect Angle	δ_1, δ_2	Aspect angle of target relative to bistatic bisector for each Transmitter-Target-Receiver bistatic system
Offset Angle	$\theta_{off1}, \theta_{off2}$	Angle that baseline for each Transmitter-Target-Receiver bistatic system makes with horizontal axis
Subtended Angle	$\theta_{R1}, \theta_{R2}, \theta_{T1R1}, \theta_{T1R2}$	Angle subtended within each bistatic triangle
Range	R_{T1}, R_{R1}, R_{R2}	Range to target
Baseline Distance	L_1, L_2	Separation between Transmitter and Receiver for each Transmitter-Target-Receiver bistatic system
Target Velocity	V	Magnitude of target's velocity

Table 2. Notations used in multistatic radar model

C. TARGET BEARING AND RANGE RELATIVE TO TRANSMITTER

In this section, the objective is to determine the position of the target relative to the transmitter. Therefore, the parameters to be determined are: target's bearing relative to the transmitter ϕ_{T1} and the target's relative range to the transmitter, R_{T1}.

From Equation (4.3), the derivation of R_{T1} can be extended in the multistatic case to include one for each of the two bistatic triangles.

$$R_T = \frac{\left(R_T + R_R\right)^2 - L^2}{2\left[\left(R_T + R_R\right) - L\sin\left(\phi_T\right)\right]} \tag{4.3}$$

For the multistatic radar model (see Figure 11), the baseline for each transmitter-receiver pair may not be aligned with the horizontal axis; hence, additional offset angles need to be considered for the correct derivation. The angle ϕ_T in the denominator of Equation (4.3) will need to include θ_{off1} and θ_{off2}.

$$R_{T1} = \frac{\left(R_{T1} + R_{R1}\right)^2 - L_1^2}{2\left(R_{T1} + R_{R1} - L_1\sin\left(\phi_{T1} + \theta_{off1}\right)\right)} \tag{5.1}$$

$$R_{T1} = \frac{\left(R_{T1} + R_{R2}\right)^2 - L_2^2}{2\left(R_{T1} + R_{R2} - L_2\sin\left(\phi_{T1} + \theta_{off2}\right)\right)} \tag{5.2}$$

With the availability of time synchronization signals, ΔT_{D1} and ΔT_{D2}, the range sums, $R_{T1} + R_{R1}$, and $R_{T1} + R_{R2}$, can be obtained as

$$R_{T1} + R_{R1} = c\Delta T_1 + L_1 \tag{5.3}$$

$$R_{T1} + R_{R2} = c\Delta T_2 + L_2 \tag{5.4}$$

Hence, by substituting Equations (5.3) and (5.4) into Equations (5.1) and (5.2), ϕ_{T1} can be estimated by the numerical solution of

$$\frac{\left(R_{T1} + R_{R1}\right)^2 - L_1^2}{2\left(R_{T1} + R_{R1} - L_1\sin\left(\phi_{T1} + \theta_{off1}\right)\right)} - \frac{\left(R_{T1} + R_{R2}\right)^2 - L_2^2}{2\left(R_{T1} + R_{R2} - L_2\sin\left(\phi_{T1} + \theta_{off2}\right)\right)} = 0 \tag{5.5}$$

Thereafter, R_{T1} can be obtained from either Equation (5.1) or (5.2).

D. TARGET BEARING AND RANGE RELATIVE TO RECEIVERS

Next, the positions of the target relative to the receivers need to be determined. The parameters of interest are: target's bearing relative to the receivers, ϕ_{R1} and ϕ_{R2} and the target's relative range to the receivers, R_{R1} and R_{R2}. After R_{T1} and ϕ_{T1} have been determined, R_{R1} and R_{R2} can be obtained by applying the cosine rule for each of the bistatic triangles. Similar to the derivations for the transmitter, the offset angles due to the different baseline positions have to be considered.

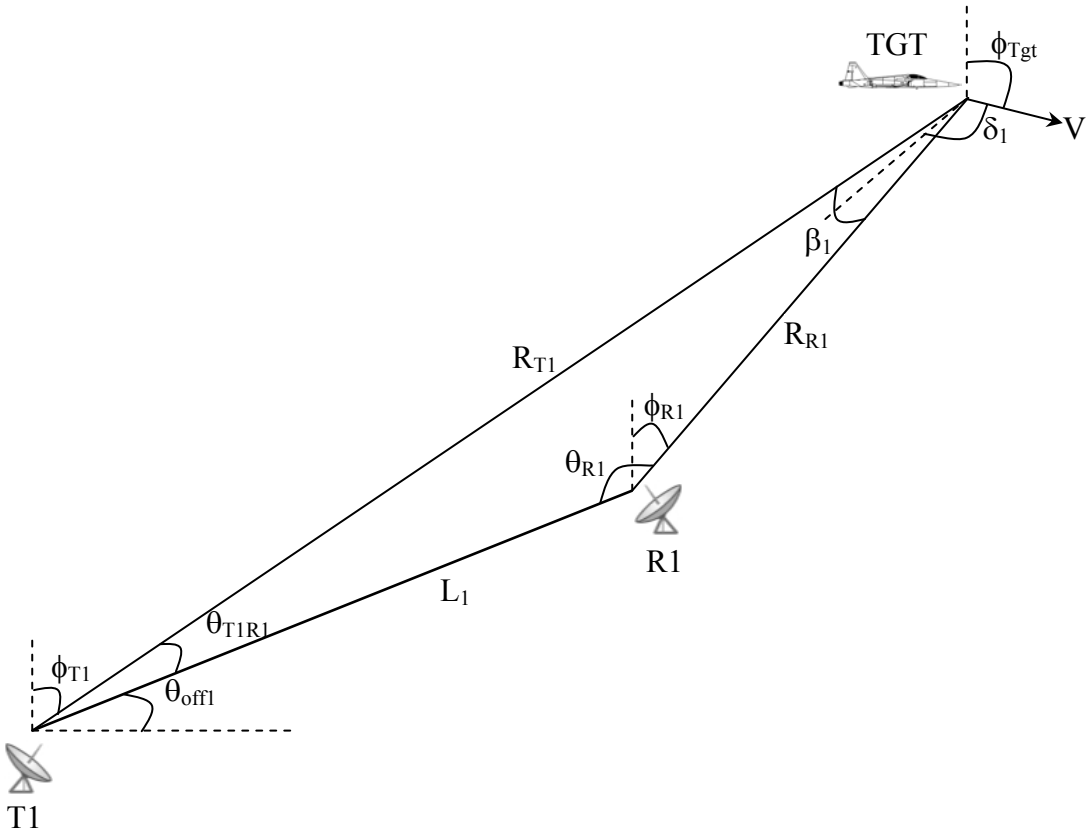

Figure 12. Bistatic triangle involving T1, R1 and TGT

For the bistatic triangle involving T1, R1 and TGT (see Figure 12), the derivation is as follows:

$$R_{R1}^2 = R_{T1}^2 + L_1^2 - 2R_{T1}L_1\cos\left(\theta_{T1R1}\right) \tag{5.6}$$

Since $\theta_{T1R1} = \frac{\pi}{2} - \phi_{T1} - \theta_{off1}$, therefore,

$$R_{R1} = \sqrt{R_{T1}^2 + L_1^2 - 2R_{T1}L_1\sin\left(\phi_{T1} + \theta_{off1}\right)} \tag{5.7}$$

Using the cosine rule, β_1 can be determined as

$$\beta_1 = \cos^{-1}\left[\frac{R_{R1}^2 + R_{T1}^2 - L_1^2}{2R_{R1}R_{T1}}\right] \tag{5.8}$$

Thereafter, by the sine rule, θ_{R1} can be derived as

$$\theta_{R1} = \sin^{-1}\left[\frac{R_{R1}\sin(\beta_1)}{L_1}\right] \tag{5.9}$$

Hence, the bearing of the target relative to receiver R1 is

$$\phi_{R1} = \phi_{T1} - \beta_1 \tag{5.10}$$

It should be noted that Equation (5.10) is only applicable in the case when the target remains on the same side of the extended baseline of the Transmitter-Receiver pair. If the target's flight path is such that it crosses to the other side of the extended baseline, then additional corrections will need to be done to obtain the correct bearing. This situation of target traversing to the other side of the extended baseline will be seen when the sum of the following angles exceed $\pi/2$.

When $\phi_{T1} + \theta_{T1R1} + \theta_{off1} > \frac{\pi}{2}$, then

$$\theta_{R1} = \pi - \theta_{T1R1} - \beta_1$$
$$\phi_{R1} = \frac{3\pi}{2} - \theta_{off1} - \theta_{R1}$$

Similarly, the parameters for second radar receiver, R2, are as follows:

$$R_{R2} = \sqrt{R_{T1}^2 + L_2^2 - 2R_{T1}L_2\sin\left(\phi_{T1} + \theta_{off2}\right)} \tag{5.11}$$

$$\beta_2 = \cos^{-1}\left[\frac{R_{R2}^2 + R_{T1}^2 - L_2^2}{2R_{R2}R_{T1}}\right] \tag{5.12}$$

$$\phi_{R2} = \phi_{T1} - \beta_2 \tag{5.13}$$

E. TARGET VELOCITY VECTOR

The target's velocity information can be extracted in two ways. Firstly, it can be obtained from the Doppler shift information picked up by the receiving stations. Secondly, with the derived target position information, a history track of the target can be maintained and the corresponding velocity vector can be derived. The required parameters are V, ϕ_{Tgt}, and either δ_1 or δ_2. The Doppler shift method will be discussed first. The amounts of Doppler shift observed by the two receiving stations are:

$$f_{D1} = \frac{2V}{\lambda}\cos(\delta_1)\cos\left(\frac{\beta_1}{2}\right) \tag{5.14}$$

$$f_{D2} = \frac{2V}{\lambda}\cos(\delta_2)\cos\left(\frac{\beta_2}{2}\right) \tag{5.15}$$

By geometry (see Figure 11),

$$\delta_1 = \delta_2 + \frac{1}{2}(\beta_2 - \beta_1) \tag{5.16}$$

Substituting δ_1 into Equation (5.14) and equating this with Equation (5.15), δ_2 can be found by the *least-squares minimization search method* such that δ_2 will minimize the following function.

$$f = \left[f_{D1}\cos(\delta_2)\cos\left(\frac{\beta_2}{2}\right) - f_{D2}\cos\left(\frac{\beta_2 - \beta_1}{2} + \delta_2\right)\cos\left(\frac{\beta_1}{2}\right)\right]^2 \tag{5.17}$$

Following that, the magnitude of the target's velocity V and its corresponding velocity direction ϕ_{Tgt} are derived.

$$V = \frac{f_{D2}\lambda}{2\cos(\delta_2)\cos\left(\frac{\beta_2}{2}\right)} \tag{5.18}$$

$$\phi_{Tgt} = \pi + \phi_{T1} - \delta_2 - \frac{\beta_2}{2} \tag{5.19}$$

It should be noted that the above equations might produce erroneous results when the target crosses to the other side of the extended baseline of the Transmitter-Receiver pair. This can be corrected by checking the magnitude of the velocity. When it becomes negative, the velocity vector direction will also have π radians of error.

THIS PAGE INTENTIONALLY LEFT BLANK

VI. RADAR MODEL IMPLEMENTATION AND RESULTS

Based on the model introduced in the previous chapter, a procedure for implementation will be described and presented in this chapter. The scenario is a straightforward test case comprising one transmitter and two receivers. The results obtained will include the target's states (location and velocity) at each time step. These will be analyzed and the errors will be examined in detail.

A. SCENARIO SETUP

Consider the case of a simple multistatic radar system comprising just one radar transmitter (T1) and two radar receivers (R1 & R2), with two airborne targets (Tgt #1 & #2) simulated to fly in different flight paths. Tgt #1 will fly in a sinusoidal path while Tgt #2 will fly in a straight line. Figure 13 shows a schematic of this configuration.

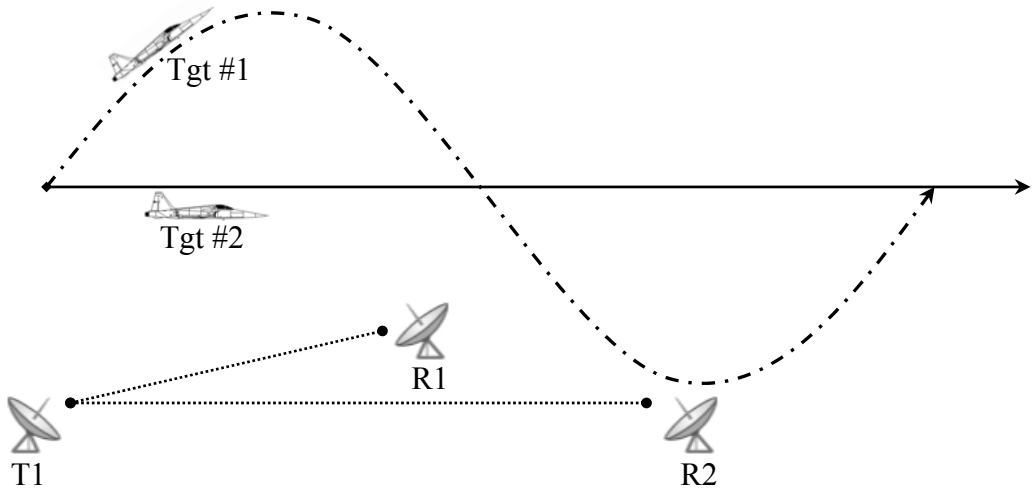

Figure 13. Plan view schematic of scenario setup

The North referenced coordinate system will be adopted for the scenario, with the origin fixed at the transmitter, T1. The coordinate positions for the transmitting and receiving stations, as well as the start positions of the airborne targets are presented in Table 3.

Entity	Position	Parameters
Transmitter (T1)	[0, 0]	-
Receiver (R1)	[50, 20]	Baseline offset: $\theta_{off1} = 21.8°$
Receiver (R2)	[100, 0]	Baseline offset: $\theta_{off2} = 0°$
Target Initial Position (Tgt #1)	[0, 100]	Velocity: $V_{1X} = 100$ m/s, $V_{2Y} = 100$ m/s
Target Initial Position (Tgt #2)	[0, 100]	Velocity: $V_{2X} = 100$ m/s, $V_{2Y} = 0$

Table 3. Radar stations and targets' disposition and other parameters

In this setup, different target flight paths and different radar transmitter-receiver baselines were tested for correctness of information extraction. T1 will transmit a CW signal at a fixed frequency of 9 GHz to simulate a band-limited system. The time step used is 1 ms and there are 3000 steps in each simulation run. This will translate to 3 seconds of target observation time.

B. TEST DATA GENERATION

For the purpose of the simulation, test data is divided into two categories: data available to the radar system and data for results comparison and analysis.

1. Data Available to Radar System

From the assumptions for this thesis research, the radar system will only have two sets of data: *synchronization time delay* and *Doppler shift*. In the simulation, these data will be generated based on the flight paths and handed over to the radar processing module to resolve the geometry and obtain accurate position and velocity details of the targets.

2. Data for Results Comparison and Analysis

The data for results comparison are tabulated in Table 4. These data are necessary to model each target at each time step.

Data	Description
Target Position	Coordinates of the target
Target Velocity	Magnitude and direction of the target
Range to T1	Range from target to transmitter (T1)
Range to R1	Range from target to receiver (R1)
Range to R2	Range from target to receiver (R2)
Bearing from T1	North referenced heading of target from transmitter (T1)
Bearing from R1	North referenced heading of target from receiver (R1)
Bearing from R2	North referenced heading of target from receiver (R2)
Bistatic Angle T1-R1	Bistatic angle for T1-Target-R1
Bistatic Angle T1-R2	Bistatic angle for T1-Target-R2
Relative Velocity from T1	Velocity component along bistatic bisector, as seen by transmitter (T1)
Relative Velocity from R1	Velocity component along bistatic bisector, as seen by receiver (R1)
Relative Velocity from R2	Velocity component along bistatic bisector, as seen by receiver (R2)

Table 4. Data for results comparison and analysis

Based on the test case, a Matlab plot of the flight paths and the radars disposition are as shown in Figure 14.

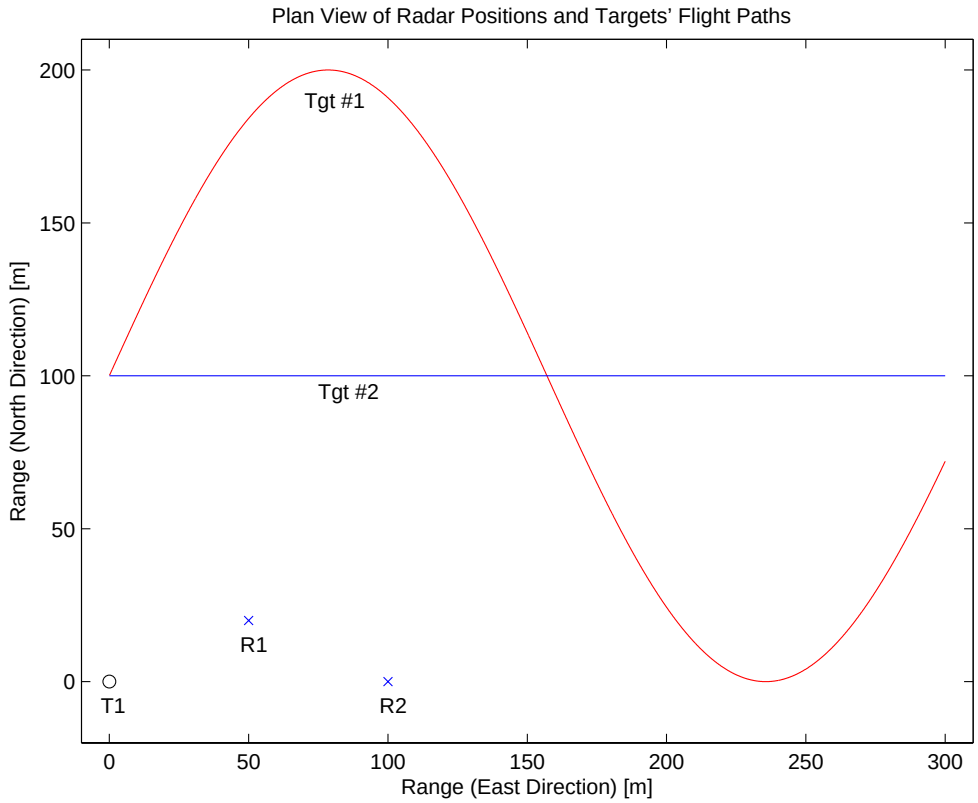

Figure 14. Radar positions and target flight paths

C. LEAST SQUARES IMPLEMENTATION

In the implementation of least squares analysis during radar measurement, the data will be collected in blocks of 5 time steps and the least squares curve fit will be done for each time block. Since each time step is 1 ms, the design matrix $\boldsymbol{A}$ employed initially to solve $\boldsymbol{Ax} = \boldsymbol{m}$ is in the form

$$\boldsymbol{A} = \begin{bmatrix} 1 & 0.001 & 0.001^2 & 0.001^3 \\ 1 & 0.002 & 0.002^2 & 0.002^3 \\ 1 & 0.003 & 0.003^2 & 0.003^3 \\ 1 & 0.004 & 0.004^2 & 0.004^3 \\ 1 & 0.005 & 0.005^2 & 0.005^3 \end{bmatrix}$$

While it may appear to be a legitimate design matrix, it is actually not suitable as it involves powers of *t* when it is a small number. This can be verified by checking the condition number for matrix ***A***.

$$cond(A) = 5.893 \times 10^{8}$$

It is clear that the condition number is large and it implies numerical instability. For example, if *cond(A)* = 10^{6}, a relative data error of the order of 10^{-6} may imply an error of 100% in the solution. Hence, matrix A is badly conditioned and its columns are nearly linearly dependent. This behavior is common, and it illustrates the importance of careful measurement acquisition. A better basis is provided by powers of a translated and scaled *t* such that

$$t' = \frac{(t - 0.003)}{0.002}$$

The value of 0.003 in the numerator is the median of the coefficients used for the cubic polynomial. The value of 0.002 in the denominator is taken to be the difference between this median value and the first coefficient value (0.001). The actual design matrix implemented and its condition number becomes

$$\boldsymbol{A'} = \begin{bmatrix} 1 & -1 & (-1)^2 & (-1)^3 \\ 1 & -0.5 & (-0.5)^2 & (-0.5)^3 \\ 1 & 0 & 0 & 0 \\ 1 & 0.5 & (0.5)^2 & (0.5)^3 \\ 1 & 1 & (1)^2 & (1)^3 \end{bmatrix} \tag{6.1}$$

$$cond(A) = 7.104$$

The resulting design is well conditioned and it is used for the analysis of position and velocity information.

D. EXTRACTION OF TARGET POSITION INFORMATION

The analysis of the signals received by the radar system will be categorized into two main areas, namely derivation of position information from the *synchronization time delay* and the extraction of velocity information from the *Doppler shift*. The derivation

of target position information will involve the determination of transmitter to receiver "round-trip" distance, target bearing and range relative to the transmitter, and target bearing and range relative to the receivers.

1. Transmitter to Receiver "Round-trip" Distance

From the synchronization time delays, the "round-trip" range from transmitter to target to receiver was first derived for each time step, target and radar transmitter-receiver pair. The range was obtained by multiplying the time delay with the speed of light and adding the baseline distance between the transmitter-receiver pair.

$$\begin{aligned}
&\text{Range T1_Tgt1_R1} = \text{Time Delay Tgt1_R1} * c + L1 \\
&\text{Range T1_Tgt2_R1} = \text{Time Delay Tgt2_R1} * c + L1 \\
&\text{Range T1_Tgt1_R2} = \text{Time Delay Tgt1_R2} * c + L2 \\
&\text{Range T1_Tgt2_R2} = \text{Time Delay Tgt2_R2} * c + L2
\end{aligned} \tag{6.2}$$

For the test case, the two targets and two transmitter-receiver pairs will involve four sets of "round-trip" ranges for time step.

2. Target Bearing and Range Relative to Receivers (R1 & R2)

With the target bearing and range relative to the transmitter known, the ranges of the target relative to the receivers were obtained from Equations (5.7) and (5.11). Next, the bistatic angles were derived from Equations (5.8) and (5.12). The bearings of the target relative to the receivers were subsequently obtained from Equations (5.10) and (5.13).

$$R_{R1} = \sqrt{R_{T1}^2 + L_1^2 - 2R_{T1}L_1 \sin\left(\phi_{T1} + \theta_{off1}\right)} \tag{5.7}$$

$$R_{R2} = \sqrt{R_{T1}^2 + L_2^2 - 2R_{T1}L_2 \sin\left(\phi_{T1} + \theta_{off2}\right)} \tag{5.11}$$

$$\beta_1 = \cos^{-1}\left[\frac{R_{R1}^2 + R_{T1}^2 - L_1^2}{2R_{R1}R_{T1}}\right] \tag{5.8}$$

$$\beta_2 = \cos^{-1}\left[\frac{R_{R2}^2 + R_{T1}^2 - L_2^2}{2R_{R2}R_{T1}}\right] \tag{5.12}$$

$$\phi_{R1} = \phi_{T1} - \beta_1 \tag{5.10}$$

$$\phi_{R2} = \phi_{T1} - \beta_2 \tag{5.13}$$

Plots of the measured values are shown in Figures 15 and 16.

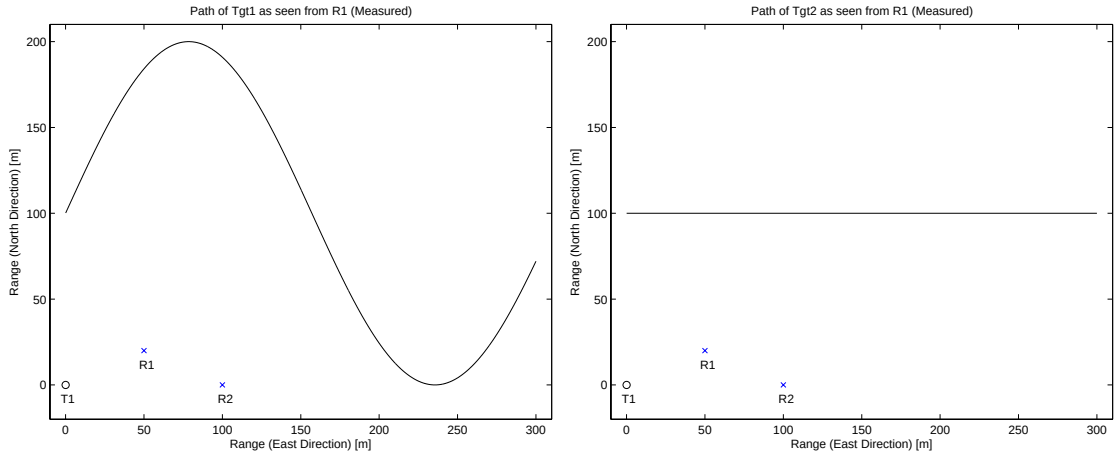

Figure 15. Plot of Tgt #1 and Tgt #2 from measured data in Receiver R1

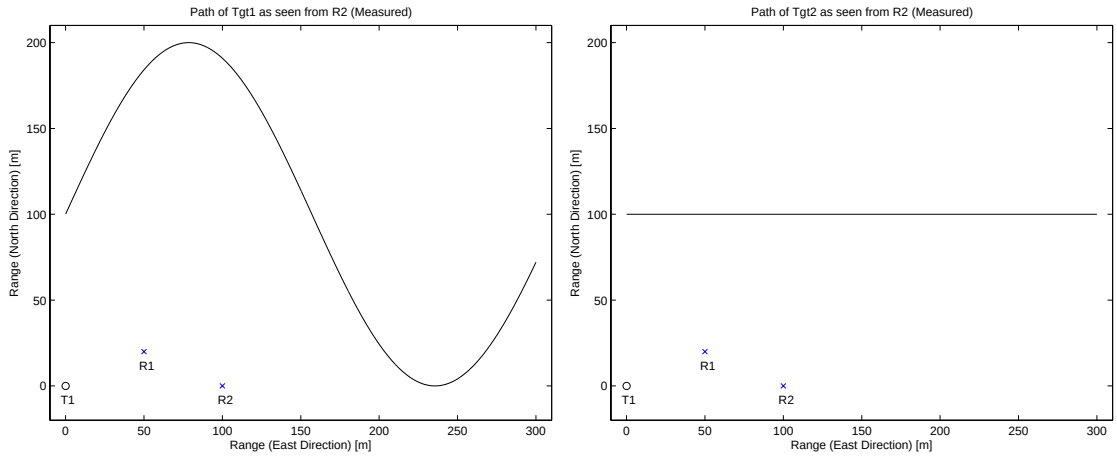

Figure 16. Plot of Tgt #1 and Tgt #2 from measured data in Receiver R2

In view of the lack of resolution in these figures, the graphical results appear to be accurate enough for imaging purposes. Upon detailed comparison of each data point, measurement errors can be calculated and analyzed. The average errors and corresponding standard deviations of the measured results are tabulated in Table 5.

Measurement Errors in Position	Receiver R1		Receiver R2	
	Avg Error	Std Dev	Avg Error	Std Dev
Range Error for Tgt 1 [m]	-1.578×10^{-13}	1.727×10^{-10}	-1.048×10^{-14}	2.214×10^{-10}
Range Error for Tgt 2 [m]	-4.597×10^{-14}	1.261×10^{-11}	1.445×10^{-14}	8.427×10^{-12}
Bearing Error for Tgt 1 [rad]	2.720×10^{-15}	2.060×10^{-12}	-7.915×10^{-13}	3.991×10^{-11}
Bearing Error for Tgt 2 [rad]	1.134×10^{-15}	3.261×10^{-13}	-2.722×10^{-16}	1.319×10^{-13}

Table 5. Average error and standard deviation in target position errors

E. EXTRACTION OF TARGET VELOCITY INFORMATION

The extraction of targets' velocity information will involve the processing of Doppler information established by receivers R1 and R2. With the Doppler information, the least-square minimization search method was adopted in Equation (5.17) to obtain the aspect angle of the target relative to the bistatic bisector.

$$f = \left[f_{D1}\cos(\delta_2)\cos\left(\frac{\beta_2}{2}\right) - f_{D2}\cos\left(\frac{\beta_2-\beta_1}{2}+\delta_2\right)\cos\left(\frac{\beta_1}{2}\right)\right]^2 \tag{5.17}$$

Thereafter, the magnitude of the target's velocity and its corresponding velocity direction were derived from Equations (5.18) and (5.19).

$$V = \frac{f_{D2}\lambda}{2\cos(\delta_2)\cos\left(\frac{\beta_2}{2}\right)} \tag{5.18}$$

$$\phi_{Tgt} = \pi + \phi_{T1} - \delta_2 - \frac{\beta_2}{2} \tag{5.19}$$

Figures 17 and 18 show the plots of the velocity magnitude and direction.

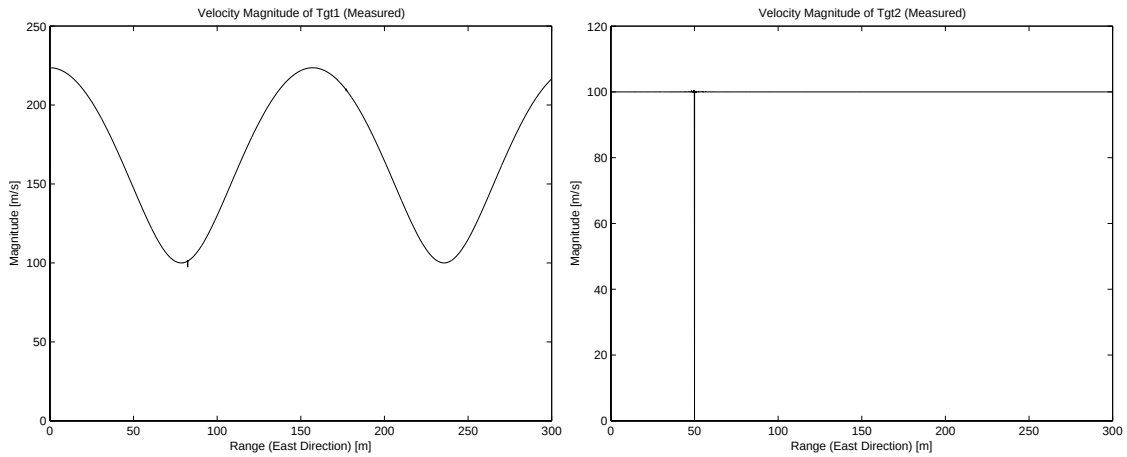

Figure 17. Velocity magnitude of Tgt #1 and Tgt #2 from measured data

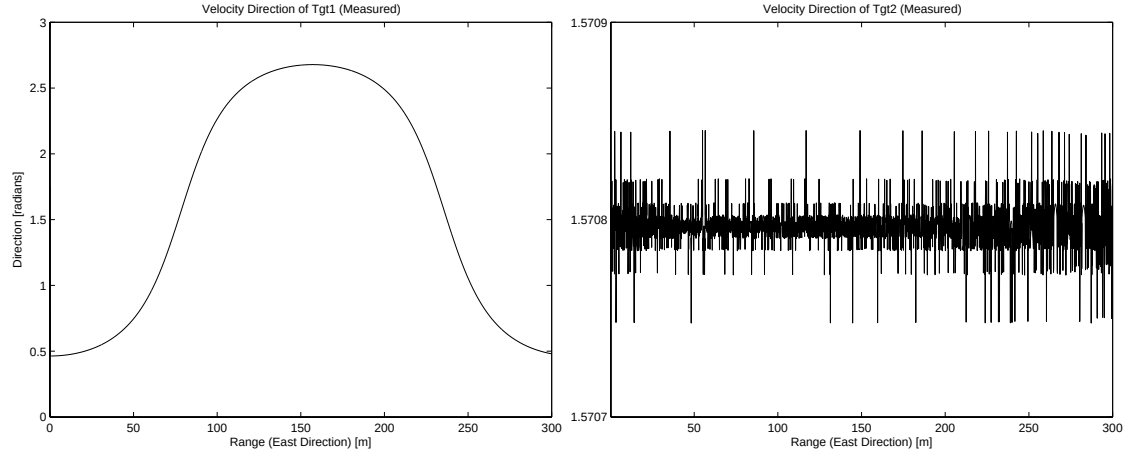

Figure 18. Velocity direction of Tgt #1 and Tgt #2 from measured data

From these figures, it may appear that errors are more pronounced in Tgt #2 as compared to Tgt #1. In reality, the errors for both targets are comparable and the discrepancy is due to the limitation of resolution of the figures. The tabulated errors for velocity magnitude and direction are tabulated in Table 6.

Measurement Errors in Velocity	Receiver R1	
	Avg Error	**Std Dev**
Magnitude Error for Tgt 1 [m/s]	-8.446×10^{-4}	0.492
Magnitude Error for Tgt 2 [m/s]	-3.297×10^{-2}	1.826
Direction Error for Tgt 1 [rad]	5.834×10^{-4}	3.174×10^{-2}
Direction Error for Tgt 2 [rad]	5.836×10^{-4}	3.190×10^{-2}

Table 6. Average error and standard deviation in target velocity errors

VII. ERROR ANALYSIS

A. OVERVIEW

The errors arising as a result of the measurements can be broadly categorized into four areas, namely *position errors* in range and bearing, and *Doppler errors* in velocity magnitude and velocity direction. For each of these categories, the relevant measurements are compared with the test data values, and the differences are treated as errors and plotted. If the errors are significant, they will be manifested in the radar image as imaging artifacts. Some of the significant errors in a noiseless environment are first analyzed. They serve to illustrate the effect of the geometry of radar systems relative to the targets. Although the measurements can be considered precise, the image errors can still be significant if the condition number for the design matrix is large. Thereafter, the errors with additive Gaussian noise are examined, so that the real world performance of the system can be better understood.

B. ERRORS IN BEARING MEASUREMENT

For Receiver R1, Figure 19 presents the errors in bearing. It is evident that a "spike" in error occurs at around 250 m. This occurrence can be explained by reviewing the flight path of the target in relation to the disposition of the radar system. The extended baseline of the transmitter-receiver pair for T1-R1 is as shown in Figure 20. It is then obvious that the "spike" occurs at the intersection of this extended baseline with the flight path of Tgt #2. This is reasonable for a bistatic radar since for the case when the target lies on the extended baseline, the bistatic angle, $\beta = 0$, and the error is maximum. A similar "spike" was also observed in the errors for Tgt #1.

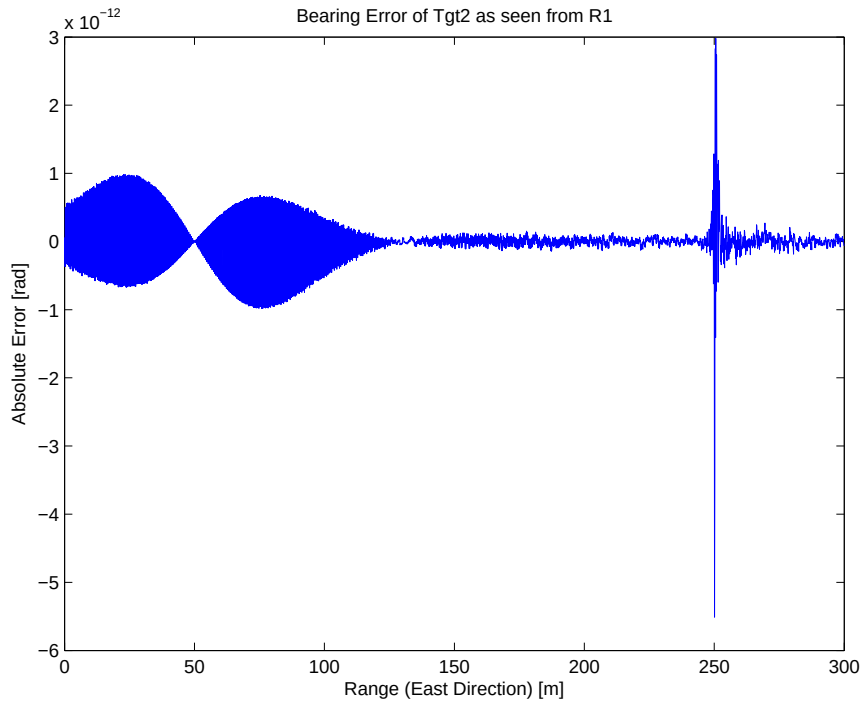

Figure 19. Bearing error for Tgt #2 as seen from receiver R1

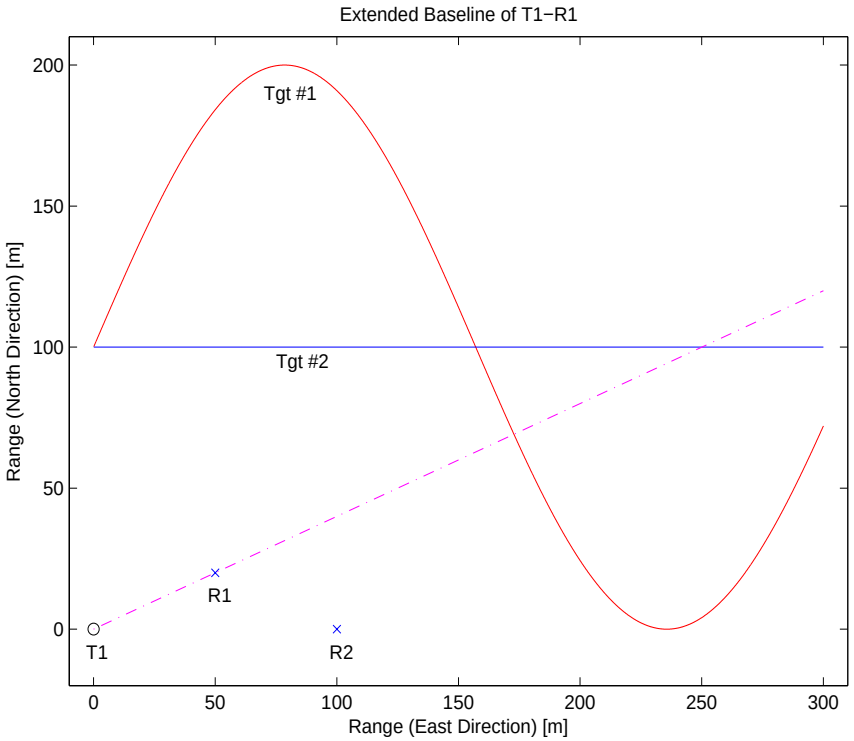

Figure 20. Extended baseline of Transmitter-Receiver pair for T1-R1

For Receiver R2, Figure 21 presents the errors in bearing. The "spike" occurs for Tgt #1 for the similar reason highlighted for Receiver R1. Figure 22 depicts the intersection of the extended baseline for Transmitter-Receiver pair T1-R2 with Tgt #1's flight path. Such "spikes" are not evident in Receiver R2 for Tgt #2 as its flight path does not intersect the extended baseline.

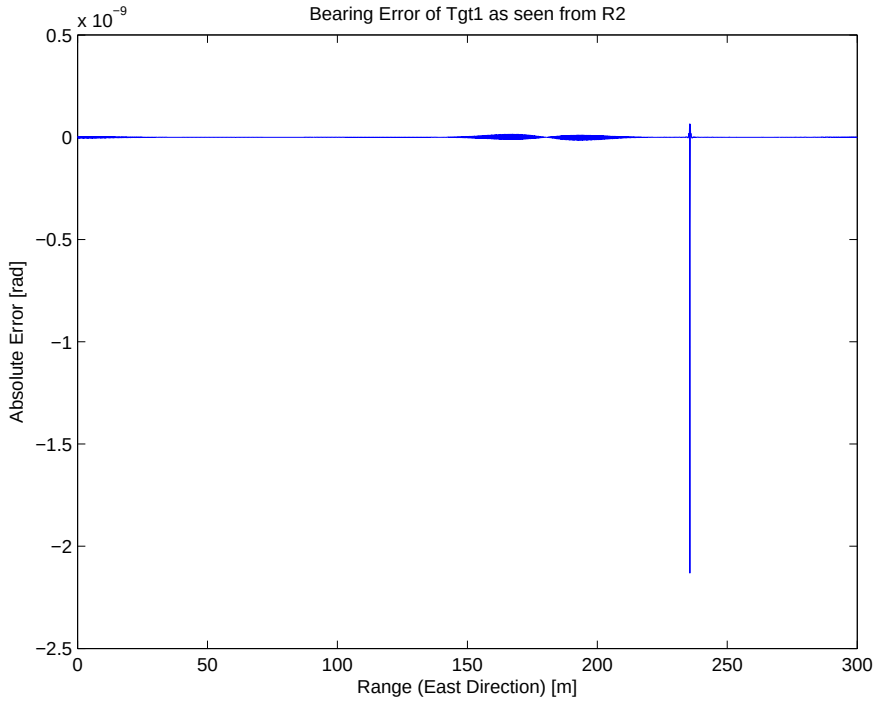

Figure 21. Bearing error for Tgt #1 as seen from receiver R2

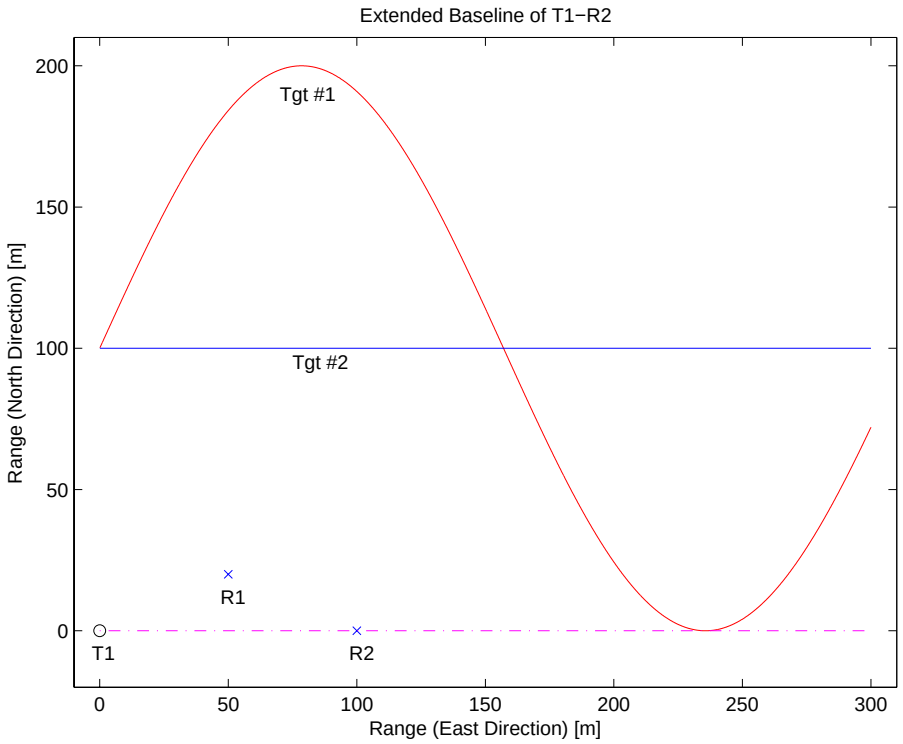

Figure 22. Extended baseline of Transmitter-Receiver pair for T1-R2

C. ERRORS IN VELOCITY MEASUREMENT

Figures 23 and 24 show the velocity magnitude errors. For Tgt #1, the error "spikes" occur at ranges of about 80 m and 175 m. The first "spike" occurred when Tgt #1 was turning back towards the South, and at about 80 m range, its aspect angle relative to the radar system was 90 degrees. Consequently, there was a transition of the radial velocity through zero and hence, there was a brief moment of zero Doppler shift. The second "spike" occurred when Tgt #1 was at the extended baseline of the Transmitter-Receiver pair T1-R1.

For Tgt #2, the error "spike" happens at about 50 m. This is a special case where the target is traveling at the perpendicular bisector of the baseline of Transmitter-Receiver pair T1-R2 with 90 degrees aspect angle. Consequently, there was zero Doppler shift and the radar system responded with a "spike". Figure 25 depicts the erroneous regions for velocity magnitude measurements.

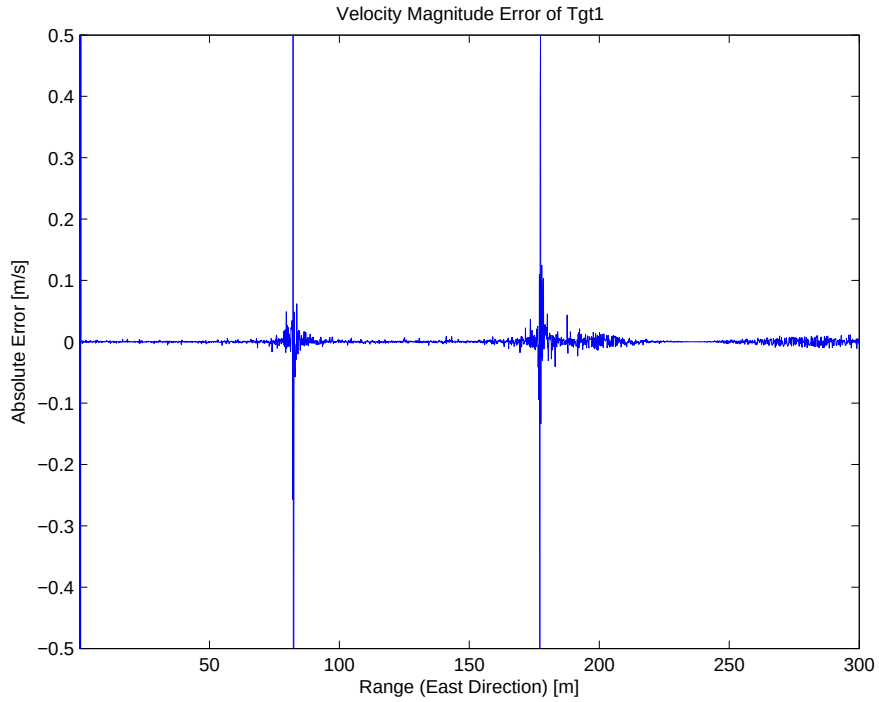

Figure 23. Velocity magnitude error for Tgt #1

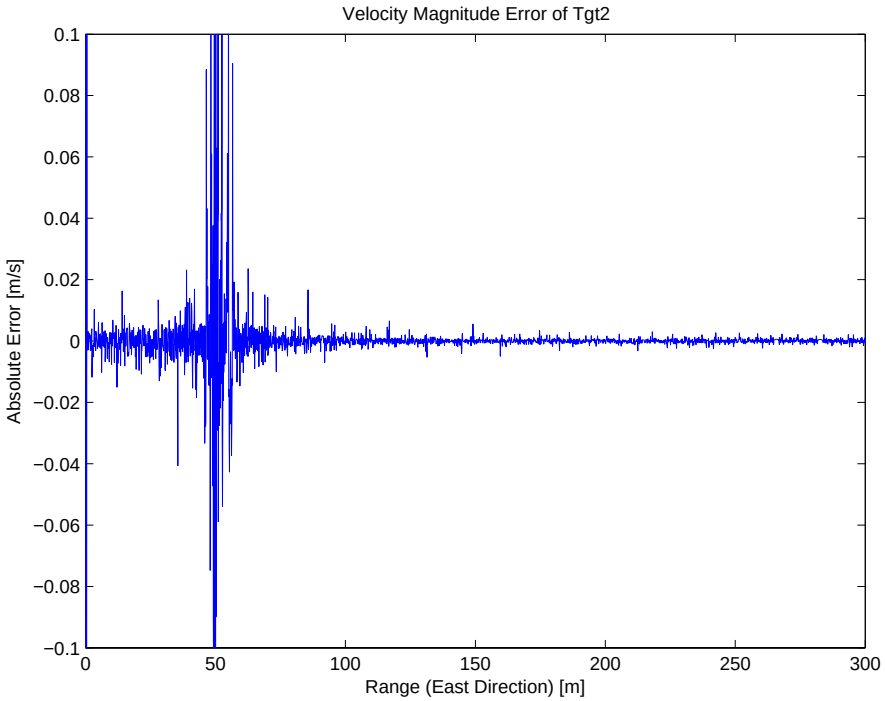

Figure 24. Velocity magnitude error for Tgt #2

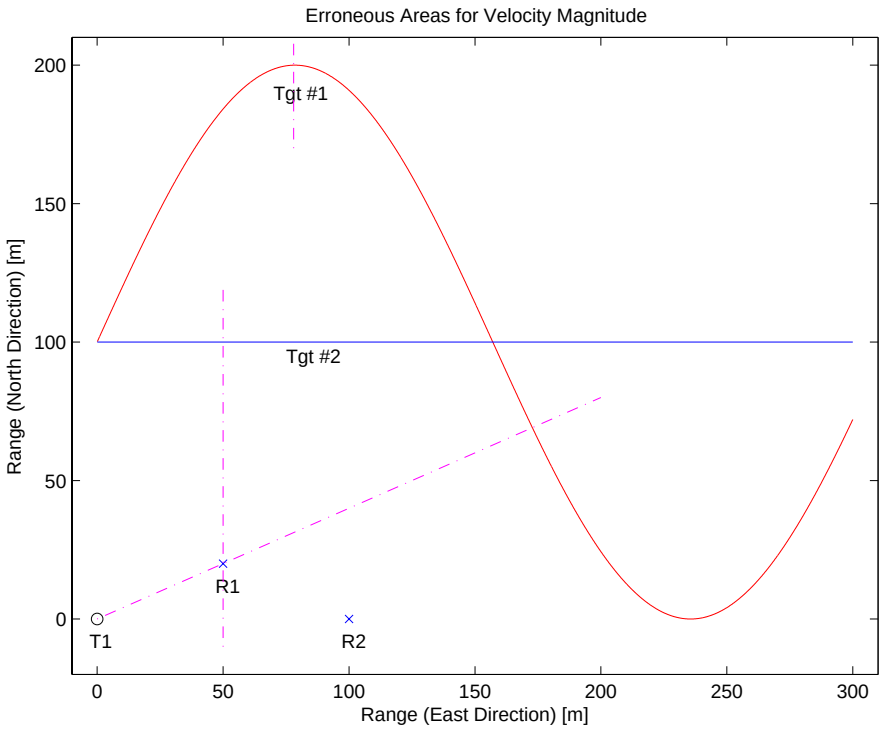

Figure 25. Erroneous regions for velocity magnitude measurements

D. ERRORS WITH ADDITIVE GAUSSIAN NOISE

For the purpose of concept demonstration, the errors analyzed so far have been based on a noiseless environment. In actual radar operations, noise is an important factor that cannot be neglected. Hence, the effect of noise on the radar model was tested with additive Gaussian noise applied onto the synchronization signal and the Doppler shifts measured by the radar system. The standard deviation used was two percent of the measured signal. Figures 26, 27, 28, and 29 present samples of the errors for Tgt #1 with additive Gaussian noise.

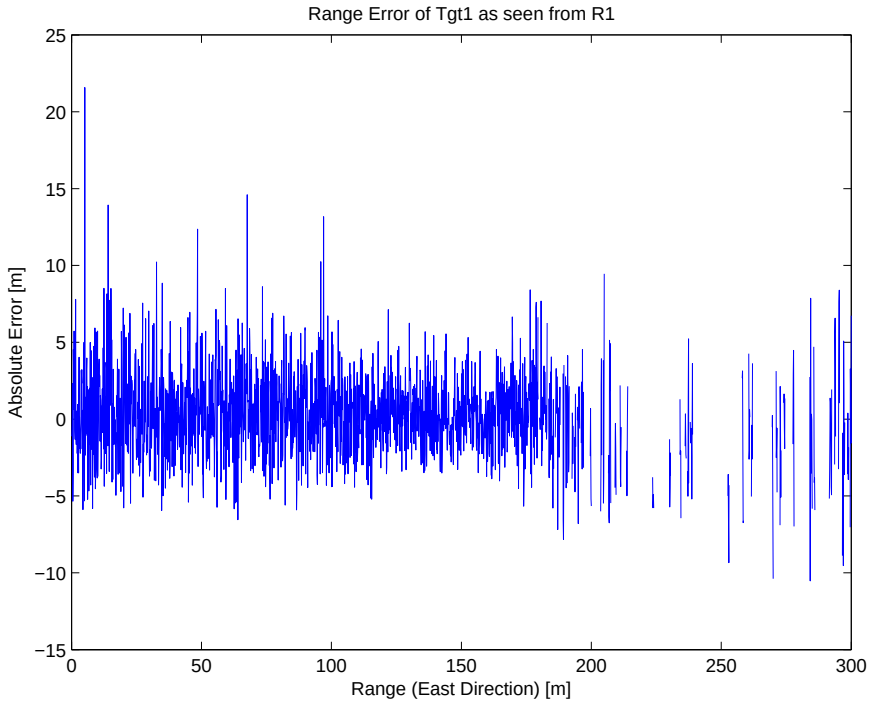

Figure 26. Range error for Tgt #1 as seen from receiver R1 (with 2% Gaussian noise)

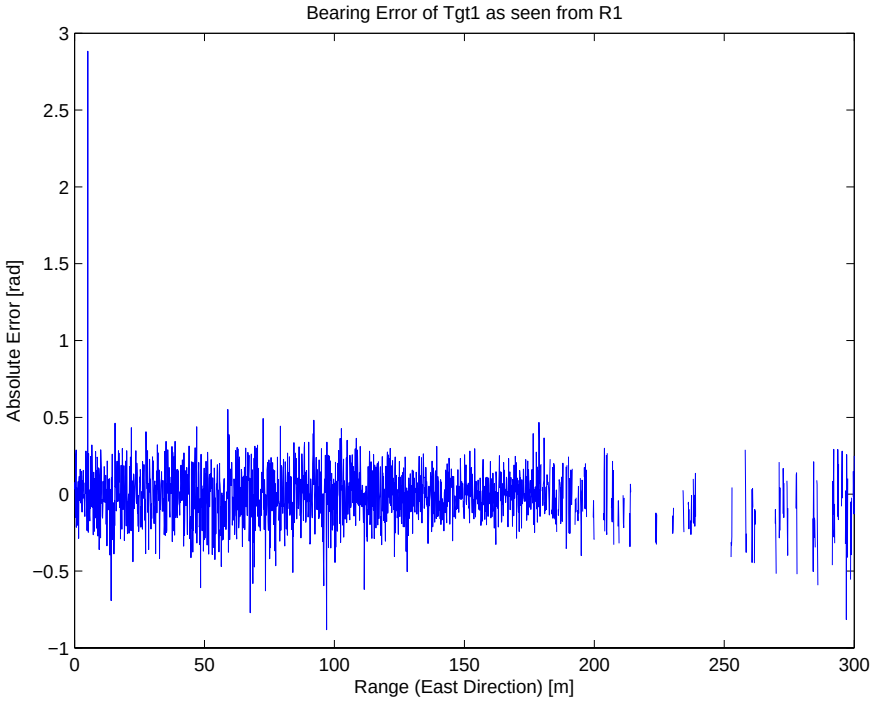

Figure 27. Bearing error for Tgt #1 as seen from receiver R1 (with 2% Gaussian noise)

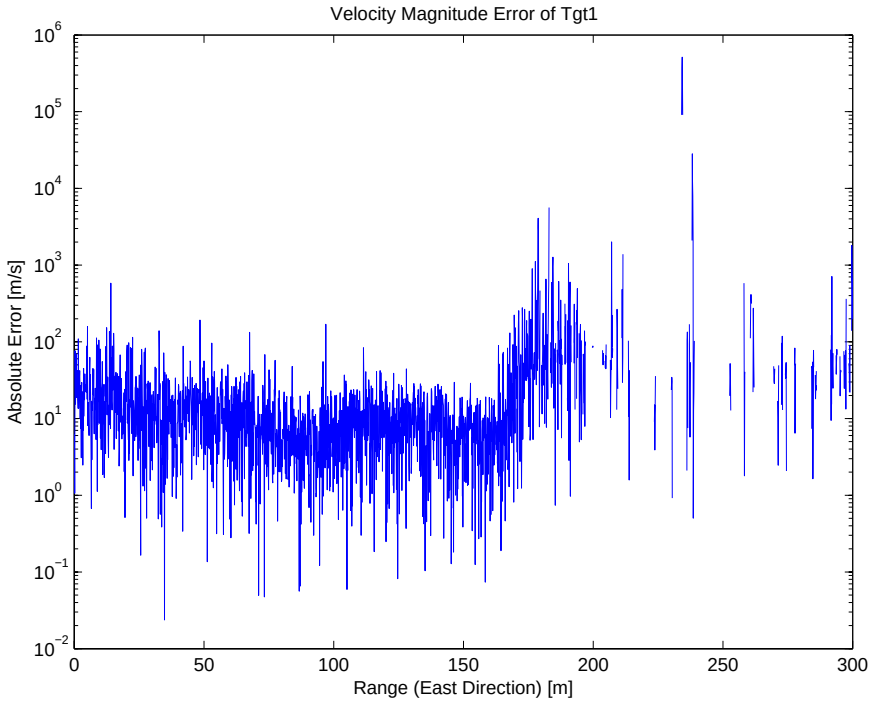

Figure 28. Velocity magnitude error for Tgt #1 (with 2% Gaussian noise)

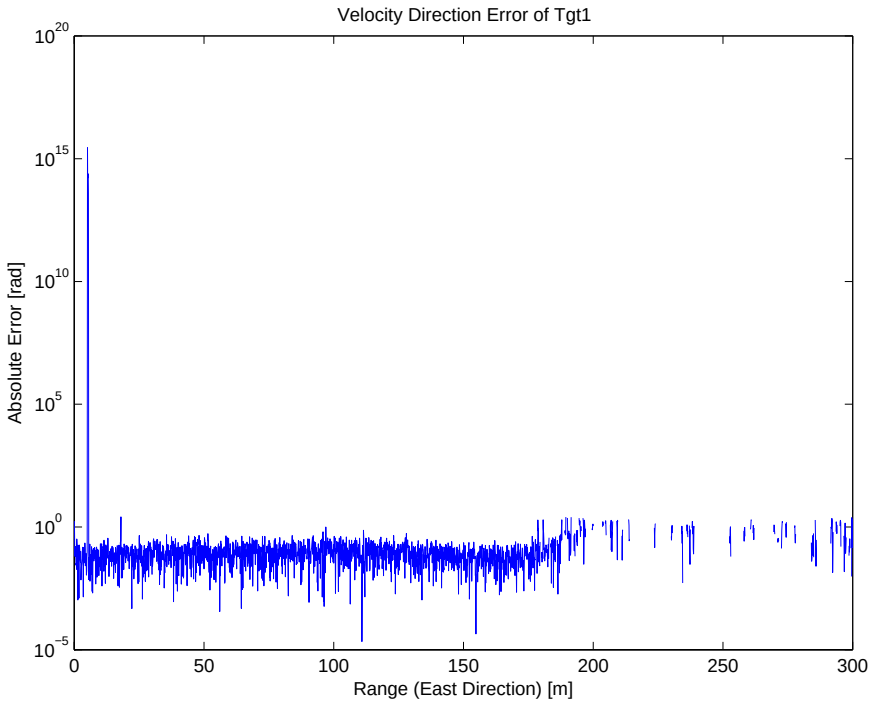

Figure 29. Velocity direction error for Tgt #1 (with 2% Gaussian noise)

It is clear that the errors are significantly more pronounced than the noiseless case. Furthermore, since the order of magnitude of the errors are larger, the error "spikes" observed in the noiseless case as a result of the target being along the extended baseline of the transmitter-receiver pair are no longer apparent. Nonetheless, these results are still accurate enough for imaging purposes.

The radar model was tested for other larger values of additive Gaussian noise. It was noted that, when the additive noise was increased to ten percent, the radar model could not provide much conclusive results. Figures 30 and 31 show the sample range and bearing errors. This was due to the use of the functions *fzero* and *fminsearch* in the Matlab code. In the simulation, these functions encountered extreme values and cannot provide reasonable solutions in the search for minimum values. The algorithms in the Matlab code will need to be refined to handle these errors.

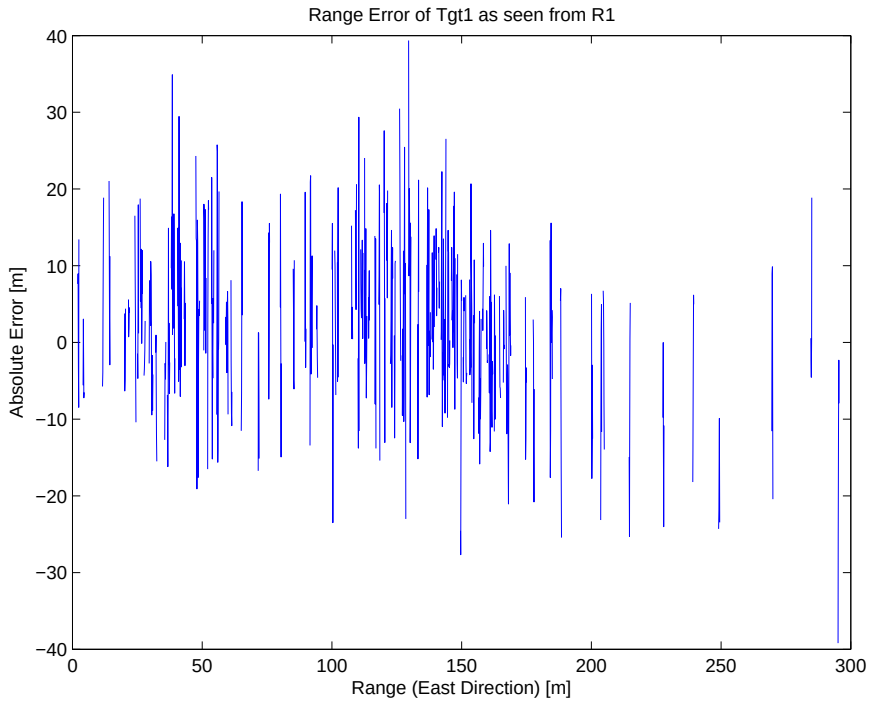

Figure 30. Range error for Tgt #1 as seen from receiver R1 (with 10% Gaussian noise)

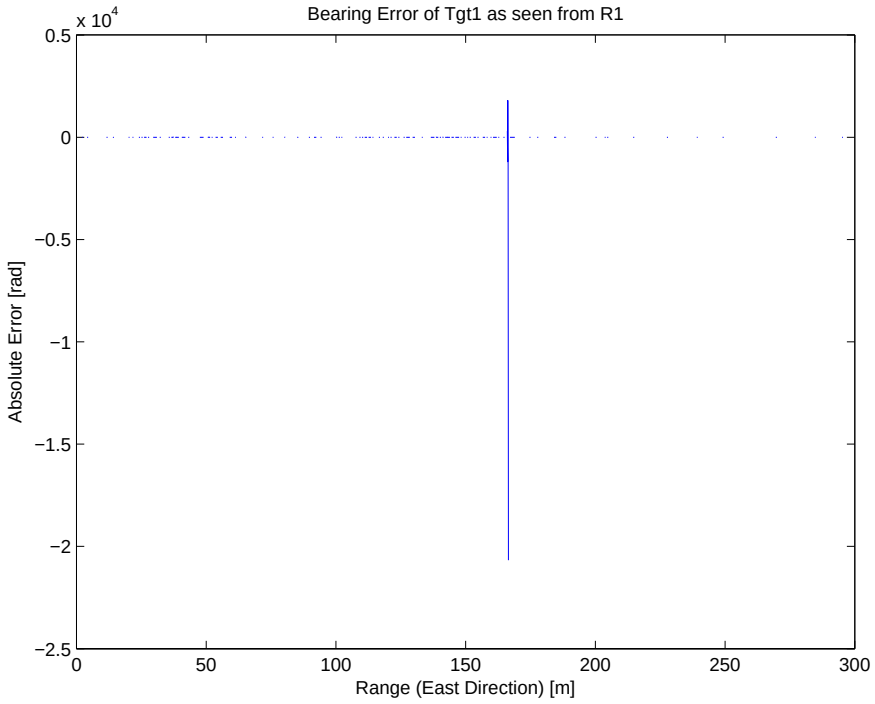

Figure 31. Bearing error for Tgt #1 as seen from receiver R1 (with 10% Gaussian noise)

Table 7 tabulates the standard deviation of the errors, taken to be the root mean square deviation from the mean, as a result of various amounts of additive Gaussian noise.

Gaussian Noise	0.2%	0.5%	1.0%	1.5%	2.0%	3.0%	4.0%	5.0%
Range	0.4122	0.9378	1.4966	2.1441	2.8388	4.1039	5.6526	6.2225
Bearing	0.0242	0.0551	429.5414	392.2657	0.2024	0.3073	439.0524	0.5210
Velocity Magnitude	373.7993	860.6418	1.5707e3	412.4362	543.7135	1.7291e13	794.3593	2.1248e4
Velocity Direction	0.3124	0.4306	429.5287	392.2597	9.5243+13	1.8549e14	3.5188e14	3.3726e14

Table 7. Standard deviation of the different types of errors for various amounts of Gaussian Noise

Figures 32, 33, 34, and 35 plot these errors as a function of the amount of Gaussian noise. It appears that the relationship between the standard deviation of range errors is approximately linear to the amount of Gaussian noise added. This is rational since the range errors are largely dependent on the errors in time synchronization only. For the remaining three aspects, namely the bearing, velocity magnitude and velocity direction errors, the coupling of the errors in the time synchronization with the errors in the Doppler frequencies will generally result in larger deviations of errors.

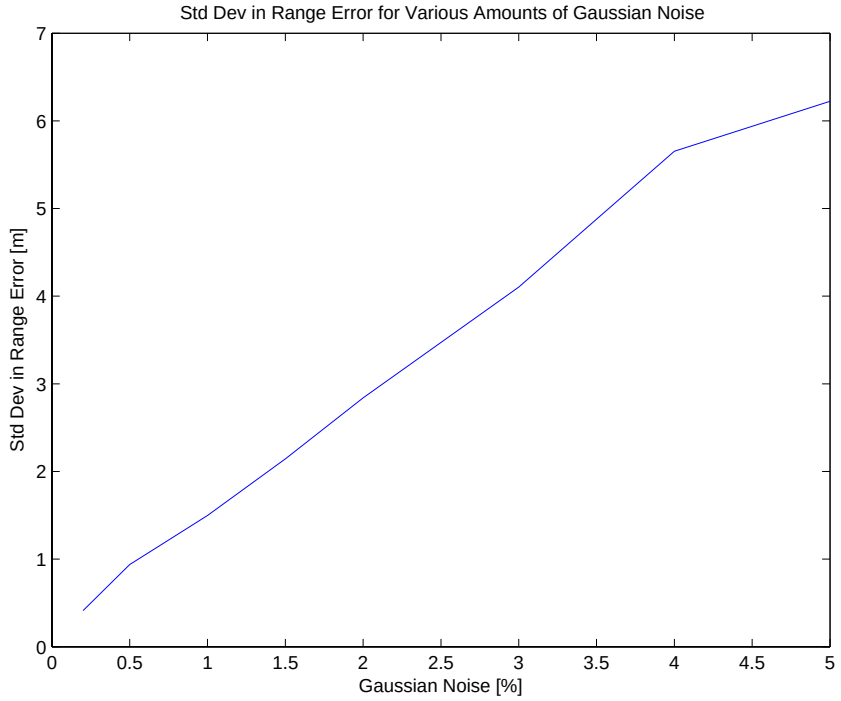

Figure 32. Standard deviation in range errors for various amounts of Gaussian noise

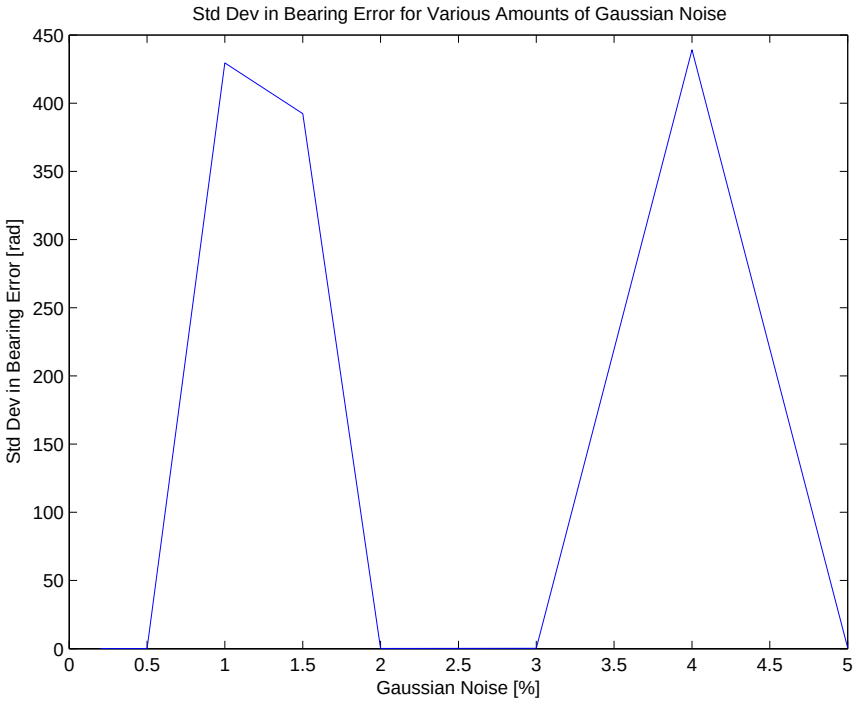

Figure 33. Standard deviation in bearing errors for various amounts of Gaussian noise

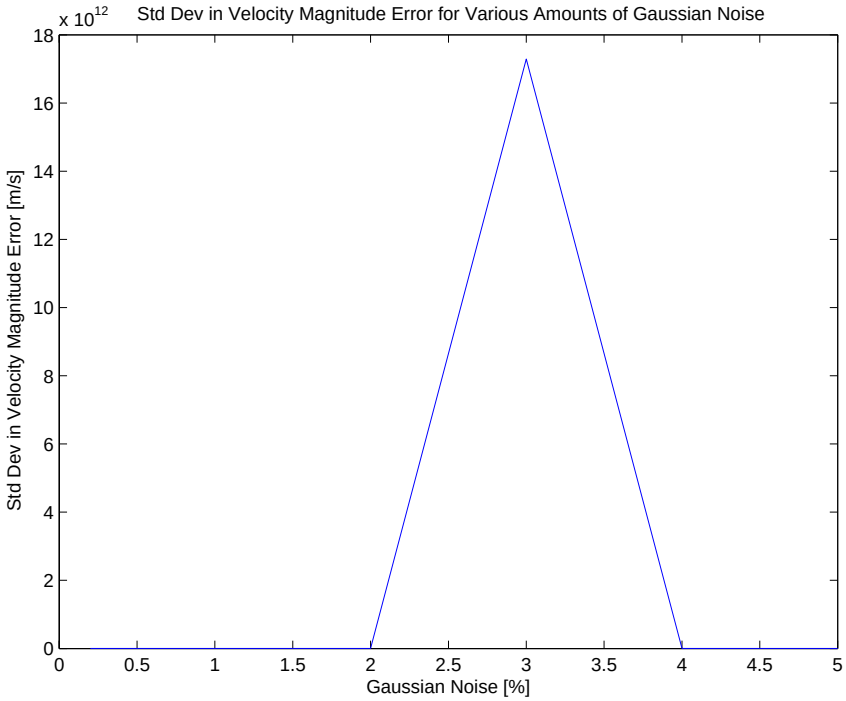

Figure 34. Standard deviation in velocity magnitude errors for various amounts of Gaussian noise

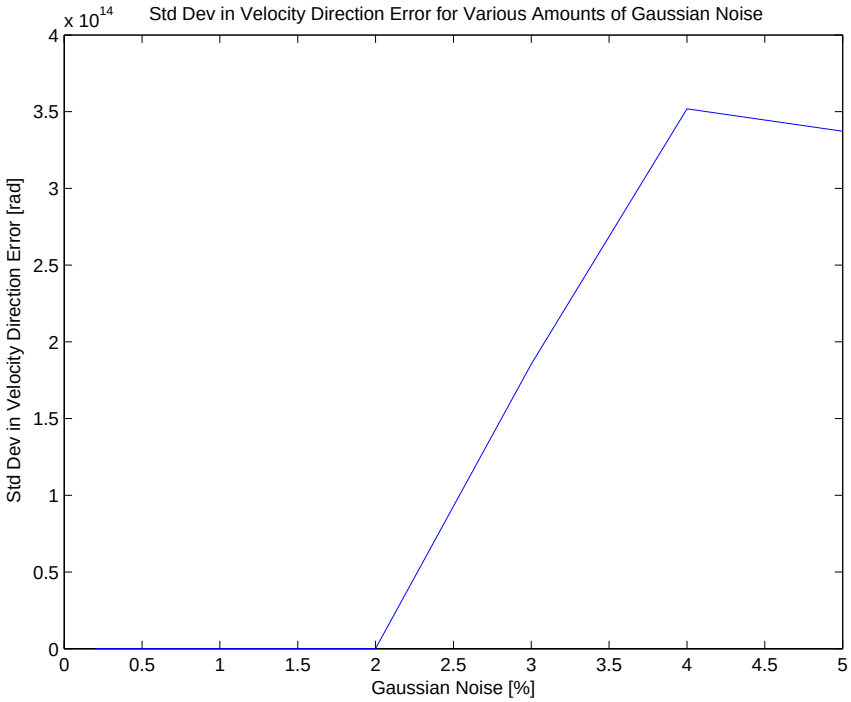

Figure 35. Standard deviation in velocity direction errors for various amounts of Gaussian noise

THIS PAGE INTENTIONALLY LEFT BLANK

VIII. RECOMMENDATIONS AND CONCLUSION

A. RECOMMENDATIONS FOR FUTURE WORK

1. More Complex Scenarios

The multistatic radar system analyzed thus far was based on the straightforward disposition of one transmitter and two receivers. Although this was adequate for the proof of concept of providing high-resolution imagery of airborne targets, the employment of more transmitting and receiving stations can support more complex treatment of image and error analysis. With more transmitter-receiver pairs, additional algorithm can be applied to eliminate the error "spikes" and imaging artifacts.

Further, the scenario was tested based on simple two-dimensional geometry. A more generalized analysis with a three-dimensional perspective could reveal issues and challenges that degrade the performance of the imaging system. For instance, due to symmetry, when conducting measurements using only Doppler information, a target trajectory cannot be distinguished from its mirror image about a vertical plane that bisects the baseline.

Consequently, as the scenario becomes more complex, the algorithm for the radar model will need to be more robust to handle the increased complexity. For instance, the limitations in the use of Matlab functions *fzero* and *fminsearch* need to be overcome to handle scenarios with greater noise interference.

2. Performance in Real World Environment

The test data and measurements made in the test cases were simulated to be in a noise-free environment. The inclusion of noise, clutter, and other environmental effects such as multipath in the simulations will allow a more realistic analysis of the system's performance. Historically, multipath effects have prevented the exploitation of systems using wide antenna beam widths for precision range instrumentation applications. Another problem unique to multistatic sytems is multistatic ghosts, which arise when using unaided multilateration techniques without transponders in a multitarget

environment [24]. These false target indications are generated when isorange contours from two targets intersect at locations where no target exists. After considering these real world effects, field testing of such a system will constitute an important component towards verifying the performance of the radar system, as only then, can it be determined whether this concept is practicable.

3. Analysis of Bistatic Ambiguity Function

Studies have shown that geometry plays an important role in the shape of the bistatic ambiguity function as the system configuration is varied. For instance, analysis in [25] has proposed algorithms to process the monostatic ambiguity function, and thereafter, extract the bistatic factors. When the bistatic ambiguity function can be determined reasonably well, the accuracy of the multistatic radar system can be evaluated. Additionally, the conditions for imaging artifacts can be better understood, and consequently, the artifacts can be eliminated more effectively.

B. CONCLUSION

The multistatic radar offers many advantages over monostatic radars in certain applications, especially since the receiving stations can be located at covert and distant sites relative to the transmitting stations. Furthermore, CW radars are relatively simple and inexpensive to employ and maintain. Hence, a notional CW multistatic radar system for high-resolution imaging was examined. This concept of using a Doppler-only multistatic radar system to provide high resolution imaging of airborne targets was demonstrated to be attainable. Through an understanding of conventional imaging techniques and formulation of the inverse problem in radar imaging, the demonstration radar model was designed to acquire an accurate position and velocity of the targets. The extraction errors resulted from the range, bearing and velocity measurements were congruent with the physical limitations of each transmitter-receiver pair. Using a multistatic system, the geometrical diversity allowed these limitations to be overcome.

APPENDIX

```
% Matlab code for analysis of
% High Doppler Resolution Imaging by Multistatic Continuous Wave Radars
% using Constructive Techniques
%
% by Wei Ting Soh

clear all;

f = 9e9;            % frequency
lambda = 3e8 / f;   % wavelength
dt = 0.001;         % time step
Steps = 3000;       % number of steps


% Information Available to Radar
%--------------------------------------------------------------------

% Radar Positions
Num_Tx = 1;         % number of transmitters
Num_Rx = 2;         % number of receivers
xy_Tx = [0 0];
xy_Rx = [50 20; 100 0];

% Angle offset for diff Tx_Rx baseline to horizon,
% and range between Tx and Rx
theta_offset = zeros(Num_Rx);   % offset angle for each baseline
L = zeros(Num_Rx);              % baseline distance

theta_offset =  atan((xy_Rx(:,2)-xy_Tx(2)) ./ (xy_Rx(:,1)-xy_Tx(1)));
L = sqrt((xy_Rx(:,2)-xy_Tx(1,2)).^2 + (xy_Rx(:,1)-xy_Tx(1,1)).^2);

% Targets
Num_Tgt = 2;                    % number of targets
xy0 = [0 100; 0 100];
v  = [100 100; 100 0];


% SET UP OF TEST CASE
%--------------------------------------------------------------------
% Data Parameters

data_xy_tgt     = zeros(Steps,Num_Tgt,2);       % position of targets at
each time step
data_range_Tx   = zeros(Steps,Num_Tgt,Num_Tx);  % range of targets to Tx
at each time step
data_bearing_Tx = zeros(Steps,Num_Tgt,Num_Tx);  % bearing of targets to
Tx at each time step
data_range_Rx   = zeros(Steps,Num_Tgt,Num_Rx);  % range of targets to Rx
at each time step
data_bearing_Rx = zeros(Steps,Num_Tgt,Num_Rx);  % bearing of targets to
Rx at each time step
data_beta       = zeros(Steps,Num_Tgt,Num_Rx);  % bistatic angle of
targets at each time step
data_velocity   = zeros(Steps,Num_Tgt,2);       % velocity magnitude and
direction of targets at each time step
data_Vr_Tx1     = zeros(Steps,Num_Tgt,Num_Tx);  % relative velocity of
targets to Tx at each time step
```

```
data_Vr_Rx      = zeros(Steps,Num_Tgt,Num_Rx);  % relative velocity of
targets to Rx at each time step

% Information available to radar system
time_delay      = zeros(Steps,Num_Tgt,Num_Rx);
% synchronization time delay from Tx to targets to Rx at each time step
fd              = zeros(Steps,Num_Tgt,Num_Rx);
% Doppler shift of targets at each time step


for k = 1:Steps;
    t = k * dt;

    for m = 1:Num_Tgt;

        % Target position
        data_xy_tgt(k,m,:) = xy0(m,:) + v(m,:) .* [t,sin(2*t)];

        % Velocity
        if k >= 2
            [theta, data_velocity(k,m,1)] = cart2pol((data_xy_tgt(k,m,1)
- data_xy_tgt(k-1,m,1))/dt,(data_xy_tgt(k,m,2) - data_xy_tgt(k-
1,m,2))/dt);

            if theta <= pi/2    % check for correct sector of velocity
direction
                data_velocity(k,m,2) = pi/2 - theta;
            elseif  (theta <= 1.5 * pi) and (theta > pi/2)
                    data_velocity(k,m,2) = theta - pi/2;
            elseif (theta <= 2 * pi) and (theta > 1.5*pi)
                    data_velocity(k,m,2) = 2.5*pi - theta;
            end;
        end;

        for n = 1:Num_Rx;

            % Relative range
            data_range_Tx(k,m,1) = sqrt((data_xy_tgt(k,m,2)-
xy_Tx(1,2))^2 + (data_xy_tgt(k,m,1)-xy_Tx(1,1))^2);
            data_range_Rx(k,m,n) = sqrt((data_xy_tgt(k,m,2)-
xy_Rx(n,2))^2 + (data_xy_tgt(k,m,1)-xy_Rx(n,1))^2);

            % Bearing (measured from North)
            data_bearing_Tx(k,m,1) = atan((data_xy_tgt(k,m,1)-
xy_Tx(1,1))/(data_xy_tgt(k,m,2)-xy_Tx(1,2)));

            if (data_xy_tgt(k,m,2)-xy_Rx(n,2)) >= 0  % Tgt is in NE/NW
quadrant
                    data_bearing_Rx(k,m,n) = atan((data_xy_tgt(k,m,1)-
xy_Rx(n,1))/(data_xy_tgt(k,m,2)-xy_Rx(n,2)));
            elseif (data_xy_tgt(k,m,1)-xy_Rx(n,1)) >= 0  % Tgt is in SE
quadrant
                data_bearing_Rx(k,m,n) = pi/2 +
atan(abs((data_xy_tgt(k,m,2)-xy_Rx(n,2))/(data_xy_tgt(k,m,1)-
xy_Rx(n,1))));
            else   % Tgt is in SW quadrant
                data_bearing_Rx(k,m,n) = - pi/2 -
atan(abs((data_xy_tgt(k,m,2)-xy_Rx(n,2))/(data_xy_tgt(k,m,1)-
xy_Rx(n,1))));
            end;

            % Beta angle
```

```
            data_beta(k,m,n) = acos((data_range_Tx(k,m,1)^2 +
data_range_Rx(k,m,n)^2 - L(n)^2) / (2 * data_range_Tx(k,m,1) .*
data_range_Rx(k,m,n)));

            % Time delay (between Tx and Rx)
            time_delay(k,m,n) = (data_range_Tx(k,m,1) +
data_range_Rx(k,m,n) - L(n)) / 3.0e8;

            % add 2% Gaussian noise to time delay
            time_delay(k,m,n) = time_delay(k,m,n) +
0.02*time_delay(k,m,n)*randn;

            % Relative velocity to Tx
            data_Vr_Tx1(k,m) = data_velocity(k,m,1) * cos(pi +
data_bearing_Tx(k,m,1) - data_velocity(k,m,2));

            % Doppler shift for Receivers
            data_Vr_Rx(k,m,n)  = data_velocity(k,m,1) * cos(pi +
data_bearing_Tx(k,m,1) - data_velocity(k,m,2) - data_beta(k,m,n));
            fd(k,m,n) = (data_Vr_Tx1(k,m) + data_Vr_Rx(k,m,n)) / lambda;

            % add 2% Gaussian noise to Doppler shift
            fd(k,m,n) = fd(k,m,n) + 0.02*fd(k,m,n)*randn;
        end;
    end;
end;

% Plot scenario setup
% figure;
%
plot(xy_Tx(1),xy_Tx(2),'kO',xy_Rx(:,1),xy_Rx(:,2),'bX',data_xy_tgt(:,1,1
),data_xy_tgt(:,1,2),'r',data_xy_tgt(:,2,1),data_xy_tgt(:,2,2),'b');
% axis([-10 310 -20 210]);
% xlabel('Range (East Direction) [m]');
% ylabel('Range (North Direction) [m]');
% title('Plan View of Radar Positions and Targets'' Flight Paths');
% text(-3,-8,'T1');
% text(47,12,'R1');
% text(97,-8,'R2');
% text(70,190,'Tgt #1');
% text(75,95,'Tgt #2');

% Show extended baseline for T1-R1 pair
% figure;
%
plot(xy_Tx(1),xy_Tx(2),'kO',xy_Rx(:,1),xy_Rx(:,2),'bX',data_xy_tgt(:,1,1
),data_xy_tgt(:,1,2),'r',data_xy_tgt(:,2,1),data_xy_tgt(:,2,2),'b');
% axis([-10 310 -20 210]);
% xlabel('Range (East Direction) [m]');
% ylabel('Range (North Direction) [m]');
% title('Extended Baseline of T1-R1');
% text(-3,-8,'T1');
% text(47,12,'R1');
% text(97,-8,'R2');
% text(70,190,'Tgt #1');
% text(75,95,'Tgt #2');
% line([0 300], [0 120],'Color','m','LineStyle','-.');

% Show extended baseline for T1-R2 pair
% figure;
%
plot(xy_Tx(1),xy_Tx(2),'kO',xy_Rx(:,1),xy_Rx(:,2),'bX',data_xy_tgt(:,1,1
),data_xy_tgt(:,1,2),'r',data_xy_tgt(:,2,1),data_xy_tgt(:,2,2),'b');
```

```
% axis([-10 310 -20 210]);
% xlabel('Range (East Direction) [m]');
% ylabel('Range (North Direction) [m]');
% title('Extended Baseline of T1-R2');
% text(-3,-8,'T1');
% text(47,12,'R1');
% text(97,-8,'R2');
% text(70,190,'Tgt #1');
% text(75,95,'Tgt #2');
% line([0 300], [0 0],'Color','m','LineStyle','-.');

% Show extended baseline for T1-R1 pair & perpendicular bisector for T1-
R2 pair
% figure;
%
plot(xy_Tx(1),xy_Tx(2),'kO',xy_Rx(:,1),xy_Rx(:,2),'bX',data_xy_tgt(:,1,1
),data_xy_tgt(:,1,2),'r',data_xy_tgt(:,2,1),data_xy_tgt(:,2,2),'b');
% axis([-10 310 -20 210]);
% xlabel('Range (East Direction) [m]');
% ylabel('Range (North Direction) [m]');
% title('Erroneous Areas for Velocity Magnitude');
% text(-3,-8,'T1');
% text(47,12,'R1');
% text(97,-8,'R2');
% text(70,190,'Tgt #1');
% text(75,95,'Tgt #2');
% line([0 200], [0 80],'Color','m','LineStyle','-.');
% line([50 50], [-10 120],'Color','m','LineStyle','-.');
% line([78 78], [170 210],'Color','m','LineStyle','-.');

% ------------------------------------------------------------------
% DATA PROCESSING AND SOLUTIONING

x_scale = [0.1:0.1:300]'; % set correct scale for x-axis when plotting

range_Tx    = zeros(Steps,Num_Tgt,Num_Tx);      % range of targets to Tx
at each time step
bearing_Tx  = zeros(Steps,Num_Tgt,Num_Tx);      % bearing of targets to
Tx at each time step
range_Rx    = zeros(Steps,Num_Tgt,Num_Rx);      % range of targets to Rx
at each time step
bearing_Rx  = zeros(Steps,Num_Tgt,Num_Rx);      % bearing of targets to
Rx at each time step
range_Tx_Rx = zeros(Steps,Num_Tgt,Num_Rx);      % round trip range from
Tx to Tgt to Rx  at each time step

%-----------------
% round trip range from Tx to Tgt to Rx

for m = 1:Num_Tgt;
    for n = 1:Num_Rx;

        % range of T1-Tgt-R1, T1-Tgt-R2
        range_Tx_Rx(:,m,n) = time_delay(:,m,n) * 3.0e8 + L(n);

    end;
end;

%-----------------
% for Tx

% output: range_Tx(k,m,n) & bearing_Tx(k,m,n)
```

```
for m = 1:Num_Tgt;
    for k = 1:Steps;

        thetaT = @(x) (range_Tx_Rx(k,m,1)^2-L(1)^2) / (2 *
(range_Tx_Rx(k,m,1) - L(1)*sin(x + theta_offset(1)))) -
(range_Tx_Rx(k,m,2)^2-L(2)^2) / (2 * (range_Tx_Rx(k,m,2) - L(2)*sin(x +
theta_offset(2))));
        bearing_Tx(k,m,1) = fzero(thetaT,0);
        range_Tx(k,m,1) = (range_Tx_Rx(k,m,1)^2-L(1)^2) / (2 *
(range_Tx_Rx(k,m,1) - L(1)*sin(bearing_Tx(k,m,1) + theta_offset(1)))) ;

    end;
end;


%----------------
% for all Rx

% output - position: range_Rx(k,m,n) & bearing_Rx(k,m,n)
%          velocity: velocity(k,m,n,2)  [magnitude & bearing]

beta     = zeros(Steps,Num_Tgt,Num_Rx);         % Bistatic angle of
targets for each Tx-Rx pair at each time step
delta    = zeros(Steps,Num_Tgt,Num_Rx);         % Delta angle of targets
for each Tx-Rx pair at each time step
velocity_dop = zeros(Steps,Num_Tgt,2);          % velocity magnitude and
direction of targets at each time step

for m = 1:Num_Tgt;
    for n = 1:Num_Rx;
        for k = 1:Steps;

            range_Rx(k,m,n) = sqrt(range_Tx(k,m,1)^2 + L(n)^2 - 2 *
range_Tx(k,m,1) * L(n) * sin (bearing_Tx(k,m,1) + theta_offset(n)));
            beta(k,m,n) = acos((range_Rx(k,m,n)^2 + range_Tx(k,m,1)^2 -
L(n)^2) / (2 * range_Rx(k,m,n) * range_Tx(k,m,1)));

            % angle Tgt-Tx_Rx
            theta_Tx_Rx = asin(range_Rx(k,m,n) * sin(beta(k,m,n)) /
L(n));

            if bearing_Tx(k,m,1) + theta_Tx_Rx + theta_offset(n) > pi/2
+ 0.000001
                theta_Rx = pi - theta_Tx_Rx - beta(k,m,n);
                bearing_Rx(k,m,n) = 1.5*pi - theta_offset(n) - theta_Rx;
            else
                bearing_Rx(k,m,n) = bearing_Tx(k,m,1) - beta(k,m,n);
            end;

            % velocity relative to each receiver

            d2 = @(x) (fd(k,m,1) * cos(x) * cos(beta(k,m,2)/2) -
fd(k,m,2) * cos(0.5*(beta(k,m,2)-beta(k,m,1))+x) *
cos(beta(k,m,1)/2))^2;

            delta(k,m,2) = fminsearch(d2,1);
            delta(k,m,1) = delta(k,m,2) + (beta(k,m,2)-beta(k,m,1))/2;

            velocity_dop(k,m,1) = fd(k,m,2) * lambda / (2 *
cos(delta(k,m,2)) * cos(beta(k,m,2)/2));
            velocity_dop(k,m,2) = pi + bearing_Tx(k,m,1) - delta(k,m,2)
- beta(k,m,2)/2;
```

```
            % process negative velocities
            if velocity_dop(k,m,1) < 0
                velocity_dop(k,m,1) = abs(velocity_dop(k,m,1));
                if velocity_dop(k,m,2) > pi
                    velocity_dop(k,m,2) = velocity_dop(k,m,2) - pi;
                end;
            end;
        end;
    end;
end;


%-----------------------------------------------------------------------
% Least square processing: Ax = B
% Error calculation

window            = 5;
soln_Range        = [];
soln_Bearing      = [];

Processed_Range   = [];
Processed_Bearing = [];
Processed_VelMag  = [];
Processed_VelDir  = [];

error_Range       = [];
error_Bearing     = [];
error_VelMag      = [];
error_VelDir      = [];

% Design matrix
A = [];
for s = 1:window;
    tt = (s*dt - 0.003) / 0.002;   % time scaling for better basis of
design matrix
    A = [A; 1 tt tt^2 tt^3];       % design matrix
end;

for m = 1:Num_Tgt;
    for n = 1:Num_Rx;

        soln_Range   = [];
        soln_Bearing = [];
        soln_VelMag  = [];
        soln_VelDir  = [];
        for l = 1:(window):3000;  % divide entire range into blocks of
'window'
            B1 = [];   % A * x1 = B1
            B2 = [];   % A * x2 = B2
            B3 = [];
            B4 = [];

            for s = 1:window;  % extract data for the window
                B1 = [B1; range_Rx(l+s-1,m,n)];
                B2 = [B2; bearing_Rx(l+s-1,m,n)];
                B3 = [B3; velocity_dop(l+s-1,m,1)];
                B4 = [B4; velocity_dop(l+s-1,m,2)];
            end;

            x1 = A * lsqr(A, B1, 1e-16);
            x2 = A * lsqr(A, B2, 1e-16);
            x3 = A * lsqr(A, B3, 1e-16);
            x4 = A * lsqr(A, B4, 1e-16);
```

```
            soln_Range = [soln_Range; x1];
            soln_Bearing = [soln_Bearing; x2];
            soln_VelMag = [soln_VelMag; x3];
            soln_VelDir = [soln_VelDir; x4];
        end;

        Processed_Range(:,m,n) = soln_Range;
        Processed_Bearing(:,m,n) = soln_Bearing;

        error_Range(:,m,n)   = soln_Range - data_range_Rx(:,m,n);
        error_Bearing(:,m,n) = soln_Bearing - data_bearing_Rx(:,m,n);

        % Receiver range/bearing errors
        figure;
        plot(x_scale,error_Range(:,m,n));
        title(['Range Error of Tgt',int2str(m), ' as seen from
R',int2str(n)]);
        xlabel('Range (East Direction) [m]');
        ylabel('Absolute Error [m]');

        figure;
        plot(x_scale,error_Bearing(:,m,n));
        title(['Bearing Error of Tgt',int2str(m),' as seen from
R',int2str(n)]);
        xlabel('Range (East Direction) [m]');
        ylabel('Absolute Error [rad]');

    end;

    Processed_VelMag(:,m) = soln_VelMag;
    Processed_VelDir(:,m) = soln_VelDir;

    error_VelMag(:,m)    = soln_VelMag - data_velocity(:,m,1);
    error_VelDir(:,m)    = soln_VelDir - data_velocity(:,m,2)


    % Doppler errors
    figure;
    plot(x_scale,error_VelMag(:,m));
    title(['Velocity Magnitude Error of Tgt',int2str(m)]);
    xlabel('Range (East Direction) [m]');
    ylabel('Absolute Error [m/s]');

    figure;
    plot(x_scale,error_VelDir(:,m));
    title(['Velocity Direction Error of Tgt',int2str(m)]);
    xlabel('Range (East Direction) [m]');
    ylabel('Absolute Error [rad]');

end;
```

LIST OF REFERENCES

[1] *IEEE Standard Radar Definitions*, IEEE Std 686-1997, September 16, New York, 1997.

[2] C. Chua, "Doppler-Only Synthetic Aperture Radar," M.S. thesis, Naval Postgraduate School, Monterey, CA, USA, 2006.

[3] B. Borden, *Radar Imaging of Airborne Targets: A Primer for Applied Mathematicians and Physicists*, Taylor & Francis, 1999.

[4] M. I. Skolnik, *Introduction to Radar Systems*, 2nd edition, McGraw-Hill, 2001.

[5] J. P. Zwart, *Aircraft Recognition from Features Extracted from Measured and Simulated Radar Range Profiles*, ASCI, The Netherlands, 2003.

[6] "Radar," class notes for PH 4274, Physics Department, Naval Postgraduate School, Summer 2007.

[7] H. Stark, *Image Recovery Theory and Application*, pp. 466-467. Academic Press Inc., US, 1997.

[8] J. B. Keller, "Inverse Problems," The American Mathematical Monthly, Vol. 83, No. 2, pp. 107-118, February 1976.

[9] M. Bertero and P. Boccacci, *Introduction to Inverse Problems in Imaging*, pp. 5-10. Institute of Physics Publishing, UK, 1998.

[10] V. Maz'ya and T. Shaposhnikova, *Jacques Hadamard, A Universal Mathematician*. American Mathematical Society and London Mathematical Society, 1998.

[11] G. E. Forsythe, M.A. Malcolm, and C. B. Moler, Computer Methods for Mathematical Computations. Prentice-Hall, New Jersey, 1997.

[12] M. Bertero and P. Boccacci, *Introduction to Inverse Problems in Imaging*, pp. 81-86. Institute of Physics Publishing, UK, 1998.

[13] A. Tarantola, *Inverse Problem Theory and Methods for Model Parameter Estimation*, p. 57. Society of Industrial and Applied Mathematics. 2005.

[14] B. Borden, "Mathematical Problems in Radar Inverse Scattering," Institute of Physics Publishing on Inverse Problems, Vol. 18, No. 1, February 2002.

[15] T. Tsao, M. Slamani, P. Varshney, D. Weiner, H. Schwarzlander, and S. Borek, "Ambiguity Function for Bistatic Radar," IEEE Trans Aerospace and Electronic Systems, Vol. AES-33, pp. 1041-1051, 1997.

[16] C. J. Baker, H.D. Griffiths, I. Papoutsis, "Passive Coherent Location Radar System. Part 2: Waveform Properties," IEE Proceedings Online No. 20045083, 2005.

[17] M. C. Wicks, B. Himed, H. Bascom, and J. Clancy, "Tomography of Moving Targets (TMT) for Security and Surveillance," presented at Advances in Sensing with Security Applications, p. 3, Il Ciocco, Italy, July 2005.

[18] M. C. Wicks, B. Himed, H. Bascom, and J. Clancy, "Tomography of Moving Targets (TMT) for Security and Surveillance," presented at Advances in Sensing with Security Applications, p. 6, Il Ciocco, Italy, July 2005.

[19] N. J. Willis, *Bistatic Radar*, 2nd Edition, pp. 119-122, Technology Service Corporation, Silver Spring, MD, 1995.

[20] M. I. Skolnik, *Radar Handbook*, 2nd Edition, McGraw-Hill, USA, 1990.

[21] V. S. Chernyak, *Fundamentals of Multisite Radar Systems*, Overseas Publishers Association, Gordon and Breach Science Publishers, Singapore, 1998.

[22] N. J. Willis, *Bistatic Radar*, 2nd Edition, pp. 86-90, Technology Service Corporation, Silver Spring, MD, 1995.

[23] N. J. Willis, *Bistatic Radar*, 2nd Edition, p. 195, Technology Service Corporation, Silver Spring, MD, 1995.

[24] N. J. Willis and H. D. Griffiths, *Advances in Bistatic Radar*, SciTech Publishing Inc., USA, 2007.

[25] M. H. Sargazi and A. Jafargholi, "Bistatic Ambiguity Function and DOA Estimation for PCL radar," presented at IEEE Asia Pacific Conference on Circuits and Systems, 2006.

INITIAL DISTRIBUTION LIST

1. Defense Technical Information Center
   Ft. Belvoir, Virginia

2. Dudley Knox Library
   Naval Postgraduate School
   Monterey, California

3. Professor James H. Luscombe
   Code PH/Lj
   Naval Postgraduate School
   Monterey, California

4. Professor Brett Borden
   Code PH/Bb
   Naval Postgraduate School
   Monterey, California

5. Professor Donald L. Walters
   Code PH/We
   Naval Postgraduate School
   Monterey, California

6. Professor Yeo Tat Soon
   Director, Temasek Defence Science Institute
   National University of Singapore
   Singapore

7. Tan Lai Poh
   Senior Admin Officer (MDTS), Temasek Defence Science Institute
   National University of Singapore
   Singapore

8. Soh Wei Ting
   Ministry of Defence
   Singapore